J. Fluid Mech. (2024), *vol*. 1000, A56, doi:10.1017/jfm.2024.912

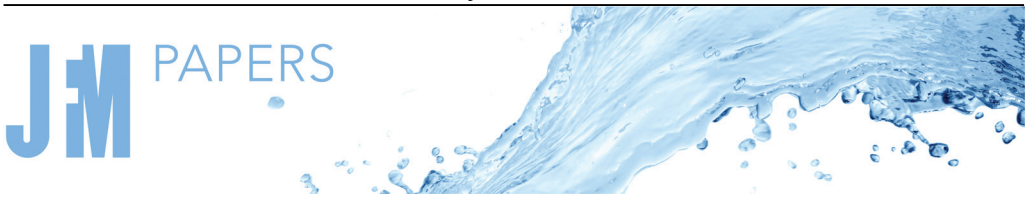

Second-order analysis of hypersonic boundary-layer stability

Francesco Grasso[1],† **and Xavier Gloerfelt**[1]

[1]DynFluid Laboratory, ENSAM, CNAM, 151 boulevard de l'Hôpital, 75013 Paris, France

(Received 15 March 2024; revised 18 September 2024; accepted 19 September 2024)

The dominant mode instability in hypersonic boundary-layer transition is the so-called second-mode instability, which has a peculiar nature strongly coupled with thermoacoustic phenomena. In linear stability theory, the unstable wave is associated with one of the two eigenvalues that originate from the acoustic branches, referred to as slow and fast modes. Interestingly, the unstable mode (slow or fast) reaches its maximum amplification as the other mode (fast or slow) attains a minimum. The phase velocity of the two modes is then very close, and this phenomenon is called synchronization. The aim of the present study is to unravel the physical mechanism that explains the second-mode growth. To that aim, second-order nonlinear equations are written for the disturbances given by linear stability. In this framework, entropy, kinetic energy and temperature energy budgets are obtained up to second order. The budgets are scrutinized for various Mach numbers and for adiabatic and cold-wall thermal conditions. Perturbation entropy budgets clearly show the process is a reversible one. An energy exchange between kinetic energy and temperature energy of the weakly nonlinear modes is driven by pressure–dilatation terms. As underlined in previous studies, the unstable mode experiences an alternate heating and cooling near the wall, which is shown to be a rather nonlinear process. The change in fluctuating thermal energy in the form of a dilatational wave is sustained by pumping disturbance kinetic energy through the pressure–dilatation term, the direction of the conversion being driven by the relative phase between pressure and dilatation. This process is similar for the slow and fast modes, the unstable mode being amplified and the other being damped. No change in the process has been noted at the location of the synchronization, suggesting that the modes have the same nature but evolve independently.

Key words: hypersonic flow, boundary layer stability

† Email address for correspondence: francesco.grasso695@gmail.com

1. Introduction

There has been a renewed interest in the understanding of supersonic and hypersonic boundary-layer aerodynamics, which is critical for the development of new generations of high-speed-flight vehicles.

1.1. *Role of pressure and dilatation in hypersonic transition*

For high-speed flows, the nature of pressure changes. Whereas it has an elliptic character in the incompressible regime and only serves to enforce a divergence-free velocity field, pressure exhibits a wave behaviour for compressible flows. This leads to a dilatational velocity component that changes the pressure–velocity interactions and affects profoundly the boundary-layer instabilities. At moderate supersonic Mach numbers, the parallel linear stability theory (LST) predicts the emergence of a first mode, which is the continuation of the viscous Tollmien–Schlichting mode. Using Lagrangian invariants, Liang *et al.* (2023) showed that the obliqueness results from the coupling of the spanwise and streamwise vorticity components. The appearance of obliqueness is accompanied by the enhancement of Reynolds shear stress (Chen, Guo & Wen 2023*b*). As the Mach number M is further increased, the velocity profile weighted by the density exhibits a generalized inflection point at a distance from the wall that increases as the Mach number increases (Lees & Lin 1946), and the first mode survives and becomes an inviscid instability. When the phase velocity becomes supersonic relative to the mean flow, typically for $M > 4$, a new region of instability appears in a higher frequency range than the first-mode instability. It corresponds to the so-called second mode that can have a high growth rate (Stetson & Kimmel 1992), except in the case of wall heating. The properties of this second mode are driven by the wave character of the pressure. This inviscid mode is associated with acoustic trapping of energy near the wall (Mack 1984; Fedorov 2011; Zhong & Wang 2012), associated with pressure–dilatation effects.

A peculiarity of hypersonic boundary layers is the possibility of multiple higher modes, which was first brought to light by Mack (1963, 1984). Similar multiple solutions were found independently by Gill (1965) for 'top-hat' jets and wakes. Morkovin (1987) explained these higher modes as sound waves reflected back and forth between the wall and the sonic line. That is why higher modes are sometimes referred to as acoustic instabilities.

Kuehl (2018) showed that the region between the wall and the sonic line behaves like an acoustic impedance well. While viscous Reynolds stress drives the Tollmien–Schlichting instability and its extension at supersonic speeds (first mode), Kuehl (2018) defined a thermoacoustic Reynolds stress that is the driving mechanism of second-mode instability. This thermacoustic interpretation also predicts the strengthening of the second mode due to wall cooling.

To shed light on the physical mechanisms at the origin of the second mode, Unnikrishnan & Gaitonde (2019) used the fluid-thermodynamic decomposition into vortical, acoustic and thermal components, initially proposed by Doak (1971, 1989) and referred to as the momentum potential theory. For hypersonic adiabatic boundary layers at M between 4 and 8, they showed, based on LST and direct numerical simulation (DNS) results, that the vorticity component for the linear second-mode instability has the highest amplitude and is concentrated in a thin layer along the critical layer. The thermal component, which is located on a thicker region centred at the same height, is the second in amplitude, whereas the acoustic mode is more spread over the boundary layer with peak values above the critical layer. Streamwise variations are significant only for the thermal and acoustic components, with an increased content just before and after

the maximum amplification of the second mode, respectively. A similar behaviour was observed for a cold-wall boundary layer and the authors concluded that the thermal and acoustic components play a primary role in the second-mode growth.

In order to explain the growth mechanisms of second-mode instability, Tian & Wen (2021) analysed the amplitude and phase of the main terms of the linear stability equations, using a relative phase analysis, similar to that used to explain the thermoacoustic coupling in a Rijke tube. The wall-normal velocity disturbances draw energy from the mean flow, which results in the growth of the second mode. The relative phase between the wall-normal fluctuations and the fluctuating internal energy in the region of the critical layer is essential in this process. Chen *et al.* (2023*b*) have extended the phase analysis of source terms to shed light on energy transfer mechanisms, explaining the features of the first mode, such as its obliqueness or the effect of wall cooling. They confirm that the driving mechanism for the second mode is a particular phase condition that allows the interaction between near-wall fluctuations and the critical layer. Chen, Guo & Wen (2023*a*) used DNS results to compare relative phase analysis with the thermoacoustic theory of Kuehl (2018) and the momentum potential theory framework. Their analysis shows that the three approaches are consistent and that the primary drivers of second-mode instability are the production of acoustic energy near the wall due to dilatational effects and its wall-normal transport to the outer region through the mean temperature gradient.

Particle image velocimetry visualizations of Zhu *et al.* (2016) at $M = 6$ revealed that the growth and decay of the second mode are accompanied by a dilatation process, and that vorticity waves developing in the critical region are synchronized. Those authors showed that the vorticity fluctuations are related to the dilatational disturbances, which yields a nonlinear resonance relation between the phase-locked travelling vorticity and dilatation waves. Zhu *et al.* (2018*a*,*b*) used experiments, LST and DNS on a flared cone at $M = 6$ to explain the presence of a heating region that occurs before the main friction heating due turbulent breakdown, and coincides with the maximum growth of the second mode. The main mechanism is associated with the pressure–dilatation term, which overwhelms the dissipation mechanism. In particular, wall heating corresponds to a peculiar phase between pressure and dilatation. Further experiments and computations by Zhu *et al.* (2020, 2021) demonstrated that the same dilatational mechanism can yield a wall cooling downstream of the heating region. They showed that the phase between pressure and dilatation can be exploited to reduce second-mode growth using a porous material.

The study of Kuehl (2018) suggests that the resonant nature of the second mode is sustained by standing acoustic waves between the wall and the sonic line. The way the acoustic waves are promoting this mode is not fully understood. Some authors (e.g. Tam & Hu 1989) propose for instance that an over-reflection, which corresponds to the amplification of an acoustic wave after reflection (Miles 1957; Ribner 1957), could be the engine of second-mode growth. Studies on over-reflection have mainly focused on geophysical applications, such as gravity waves. Recently, Zhang, Görtz & Oberlack (2022) predicted the over-reflection of acoustic waves in a supersonic exponential boundary layer. They underlined that the critical layer plays an important role in the energy exchange between waves and shear flows. The exact role of acoustic waves in hypersonic boundary-layer instabilities remains an open question.

1.2. *Synchronizations and interactions of instabilities*

A particular result of LST for hypersonic boundary layers is the presence of several eigenvalues (modes). Their origin has been clarified by Fedorov & Khokhlov (2001),

Ma & Zhong (2003*a*) and Fedorov & Tumin (2011) and we follow their terminology in the present study. Another peculiar feature of LST is the identification of various synchronization regions for these modes (Fedorov 2011; Zhong & Wang 2012). The first synchronization, from which the mode names are derived, occurs at the leading edge, where the modes are seen to leave the continuous acoustic branches. The mode leaving the slow (fast) acoustic branch is called mode S (mode F), having a phase speed equal to that of the slow (fast) acoustic mode at zero frequency $c_\varphi = 1 - 1/M$ ($c_\varphi = 1 + 1/M$). In Mack's terminology, the first mode corresponds to an extension of the Tollmien–Schlichting mode, which is a viscous instability and originates from mode S in an eigenvalue spectrum. The second mode, which appears at hypersonic speeds, is rather inviscid and driven by acoustic waves. It is most often a continuation of mode S, but can also originate from mode F. The second synchronization occurs when mode F crosses the entropy/vorticity continuous branch. This corresponds to a sudden jump in the growth rate (as clearly visible in figure 1(*c*) of § 4.1). This discontinuity would not be present using DNS or parabolic stability equations (PSE), and is rather a mathematical artefact of the eigenvalue problem with Dirichlet free-stream boundary conditions. This results in the presence of continuous branches (Balakumar & Malik 1992), and formally mode F corresponds to another eigenvalue after branch crossing. Fedorov & Tumin (2011) show that a bi-orthogonal eigenvalue expansion (Tumin 2007, 2020), which includes, in addition to mode F, an infinite number of modes belonging to the continuous spectrum of LST, can resolve this inconsistency. Further downstream, a striking result of LST is that the maximum of amplification of the second mode (S or F) corresponds to a minimum of amplification for the other mode (F or S). During this opposite amplification, the wavenumbers and phase speeds (c_φ) of the two modes are almost equal, and the slope of c_φ for mode S can exhibit an inflection to follow that of mode F (see figure 1*b*,*d*,*f*,*h* of § 4.1). This phenomenon, referred to as the FS synchronization, remains a mystery. Fedorov & Khokhlov (2001) suggested an analytical model within the two-mode approximation, involving the sum of modes F and S with a particular branching dispersion relation. Taking into account the weakly non-parallel effects, they derived a rule for the intermodal exchange, explaining why mode S or F is unstable after the branching. An important conclusion from the discrete mode branching model is that the streamwise dependence of the base flow and of the amplitude function of the normal modes (eigenfunctions), which are neglected in a parallel theory, plays an important role for the intermodal exchange. It is worth noting that linear PSE (LPSE) calculations (Lifshitz, Degani & Tumin 2012), which also take non-parallel effects into account, give a regular mode evolution in accordance with DNS results (Ma & Zhong 2003*a*). If discrete normal modes S and F are prescribed as inflow disturbances in LPSE, they evolve towards the same solution in the branching region, which correspond to the unstable mode F or S (see results of LPSE from Lifshitz *et al.* (2012) in figure 1*e*,*g* of § 4.1). It was concluded that LPSE or DNS do not exhibit a FS synchronization, and, due to mode coalescence, high streamwise gradients observed in the mode branching model of Fedorov & Khokhlov (2001) are absent in LPSE. A conjecture made by Lifshitz *et al.* (2012) is that the second synchronization (F crossing the entropy/vorticity branch) can alter the FS synchronization because there is no longer a clear separation of the branching region from the continuous spectrum, and a complete model should include the continuous branch modes in addition to discrete F and S modes. Unfortunately, the eigenfunction expansion method is not applicable when branching of modes happens. It is thus not clear if the FS synchronization, not observed in LPSE and DNS, is the result of LST approximation rather than a physical feature. Nichols & Candler (2019) used an input–output optimization to maximize the growth of second

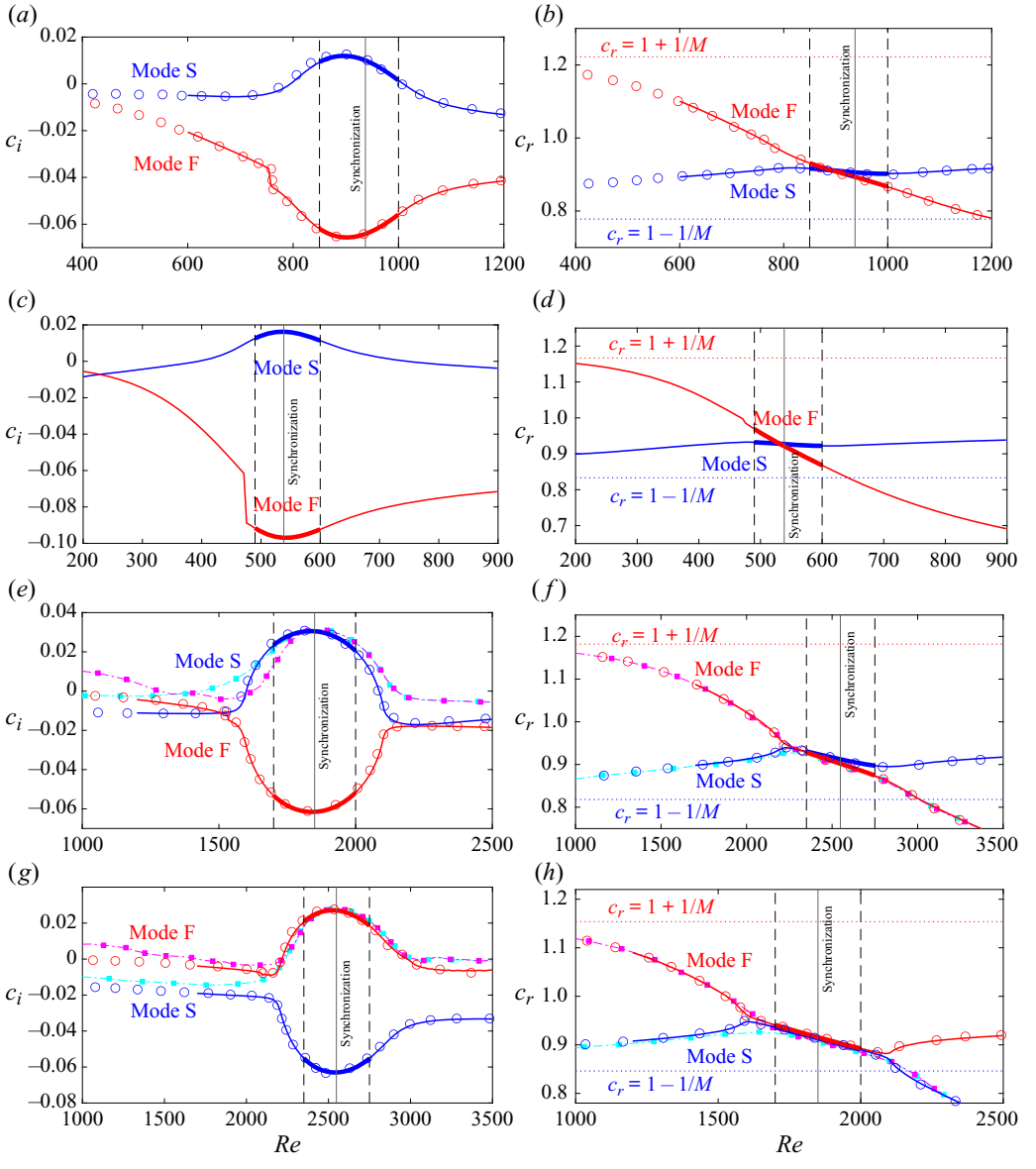

Figure 1. Phase speed as a function of Re at various Mach numbers: solid lines, present results; symbols, results from the literature (open symbols, LST from Ma & Zhong (2003*a*) for $M = 4.5$, and Fedorov & Tumin (2011) for $M = 5.5$ and $M = 6.5$; filled symbols, PSE from Lifshitz *et al.* (2012) for $M = 5.5$ and $M = 6.5$). (*a*,*c*,*e*,*g*) c_i (growth rate); (*b*,*d*,*f*,*h*) c_r. The adiabatic wall results are displayed in (*a*,*b*) ($M = 4.5$) and (*c*,*d*) ($M = 6$); (*e*,*f*) ($M = 5.5$) and (*g*,*h*) ($M = 6.5$) refer to the cold-wall cases. The solid vertical lines denote the location of the so-called FS synchronization.

mode for a cold-wall boundary layer at $M = 6.5$. They found a substantial amplification gain when both modes S and F are introduced at the inflow. Their linearized Navier–Stokes simulations thus show a coupling phenomenon, which could be associated with an FS synchronization.

Ma & Zhong (2003*a*,*b*) found that synchronization location and wave energy transfer play an important role in receptivity mechanisms. Though mode F (or mode S) may be linearly stable, it can have resonant interactions (synchronization) with both acoustic waves and the unstable mode S (or mode F). Zhu *et al.* (2016) and Chen, Zhu & Lee (2017) also observed that modal interactions, between the second mode and the first mode, Görtler instabilities, or low-frequency content, have a catalytic impact on second-mode transition to turbulence.

1.3. *Scope of the study*

The primary goal of the study is to shed some light on the physical energy transfer mechanisms and the role of the initially unstable mode (either slow or fast) at hypersonic Mach number and for both adiabatic and cold-wall thermal conditions. For the analysis focusing on the early stages of laminar-to-turbulent transition, we develop a weakly nonlinear formulation following the work of Chu & Kovasznay (1958). To account for non-parallel effects that were shown to be important by Fedorov & Khokhlov (2001) for the intermodal exchange between slow and fast modes, the formulation accounts for non-parallel effects by considering the boundary-layer growth and the corresponding streamwise derivatives. The compressible Navier–Stokes equations are briefly recalled in § 2. The second-order nonlinear disturbance equations are developed in § 3 and the stability analysis is discussed in § 4 for various Mach numbers. In an attempt to understand the role played by the energy transfer mechanisms, both reversible and irreversible, between the perturbation kinetic energy (k) and the temperature perturbation energy (k_T), in § 5 we develop the governing equations for the perturbation energies and for the perturbation entropy. Results are discussed in § 6, and conclusions of the study are given in § 7.

2. Governing equations

The conservation equations for high-Mach-number flows are written in Cartesian coordinates assuming a perfect gas and neglecting high-temperature effects. In divergence form they are

$$\frac{\partial \rho}{\partial t} + \frac{\partial J_j}{\partial x_j} = 0, \tag{2.1a}$$

$$\frac{\partial (\rho u_i)}{\partial t} + \frac{\partial (J_j u_i)}{\partial x_j} = -\frac{\partial p}{\partial x_i} + \frac{\partial \sigma_{ij}}{\partial x_j}, \tag{2.1b}$$

$$\frac{\partial (\rho T)}{\partial t} + \frac{\partial (J_j T)}{\partial x_j} = -\frac{p}{c_v}\frac{\partial u_j}{\partial x_j} + \frac{\gamma}{Pr}\frac{\partial}{\partial x_j}\left(\mu \frac{\partial T}{\partial x_j}\right) + \frac{1}{c_v}\rho\phi, \tag{2.1c}$$

$$p = \rho R T, \tag{2.1d}$$

where R is the gas constant and $\gamma = 1.4$ is the ratio of the specific heat coefficients at constant pressure (c_p) and constant volume (c_v); J_j, σ_{ij} and ϕ stand, respectively, for the jth convective flux component, the components of the stress tensor and the viscous

dissipation:

$$J_j = \rho u_j, \tag{2.2a}$$

$$\sigma_{ij} = \mu\left(2S_{ij} - \frac{2}{3}S_{\ell\ell}\delta_{ij}\right), \tag{2.2b}$$

$$S_{ij} = \frac{1}{2}\left(\frac{\partial u_i}{\partial x_j} + \frac{\partial u_j}{\partial x_i}\right), \tag{2.2c}$$

$$\phi = \frac{1}{\rho}\sigma_{ij}S_{ij}, \tag{2.2d}$$

S_{ij} being the symmetric strain tensor component and δ_{ij} the Kronecker delta. Sutherland's law is used for the viscosity μ and a constant Prandtl number $Pr = 0.72$ is assumed.

3. Second-order nonlinear disturbance equations

Linear stability analysis relies on the assumption that for a generic disturbance, the flow variables can be decomposed in a basic state plus a disturbance, where the former is assumed to be a steady-state solution of the conservation equations. Substituting such a decomposition into the governing equations leads to a linearized set of equations that describe the evolution of the disturbances. By such an approach the fundamental physical mechanisms of stability in the very early stages of disturbance evolution have been elucidated. However, because of the founding assumption that disturbances are linearly independent, the interactions between disturbances cannot be considered. This is a major drawback, since disturbance interactions are responsible for nonlinear energy transfer mechanisms and for disturbance growth leading to turbulence transition. In the present study, we introduce a decomposition of the flow variables up to second order and account for the interactions between first- and second-order perturbations by developing a weakly nonlinear analysis following the work of Chu & Kovasznay (1958).

Let q stand for either the velocity or the temperature, its instantaneous governing equation being cast in the form

$$\frac{\partial(\rho q)}{\partial t} + \frac{\partial(J_j q)}{\partial x_j} = R_q, \tag{3.1}$$

where, for brevity, R_q stands for the right-hand-side operator, whose expression is readily obtained from (2.1*b*)–(2.1*c*) and (2.2*b*)–(2.2*d*).

The weakly nonlinear governing equations are derived by introducing the following decomposition:

$$q = \bar{q} + \epsilon q' + \epsilon^2 q'', \tag{3.2}$$

where $\bar{q}$, q' and q'' represent, respectively, the base flow value and the first- and second-order disturbances of any variable q, and ϵ is a small positive number.

Substituting (3.2) in (3.1) and combining terms of the same order, the governing equations for the base flow (that are given in Appendix A) and for the first- and second-order disturbances are obtained.

3.1. *Governing equations for first-order disturbances*

The non-divergence form of the governing equations for the first-order disturbances q' is obtained by combining the following equations:

$$\frac{\partial \bar{\rho}}{\partial t} + \frac{\partial \bar{J}_j}{\partial x_j} = 0, \tag{3.3a}$$

$$\frac{\partial \rho'}{\partial t} + \frac{\partial J'_j}{\partial x_j} = 0, \tag{3.3b}$$

$$\frac{\partial}{\partial t}(\bar{\rho}q' + \rho'\bar{q}) + \frac{\partial}{\partial x_j}(\bar{J}_j q' + J'_j \bar{q}) = R'_q, \tag{3.3c}$$

thus yielding

$$\bar{\rho}\frac{\partial q'}{\partial t} + \bar{J}_j \frac{\partial q'}{\partial x_j} = R'_q - J'_j \frac{\partial \bar{q}}{\partial x_j}, \tag{3.4}$$

where $\bar{J}_j$, J'_j and R'_q are, respectively, the base flow convective flux component, the first-order convective flux component and the first-order right-hand-side operator defined as

$$\bar{J}_j = \bar{\rho}\bar{u}_j, \tag{3.5a}$$

$$J'_j = \rho'\bar{u}_j + \bar{\rho}u'_j, \tag{3.5b}$$

$$R'_q = R_{q'} = R_q(\bar{q}, \bar{\rho}, \ldots; q', \rho' \cdots). \tag{3.5c}$$

3.2. *Governing equations for second-order disturbances*

The governing equations for the second-order disturbances are derived following the same procedure. In non-divergence form, the equation for the generic second-order disturbance q'' is readily obtained by combining the base flow, first- and second-order continuity equations and the conservation equation for q'':

$$\frac{\partial \bar{\rho}}{\partial t} + \frac{\partial \bar{J}_j}{\partial x_j} = 0, \tag{3.6a}$$

$$\frac{\partial \rho'}{\partial t} + \frac{\partial J'_j}{\partial x_j} = 0, \tag{3.6b}$$

$$\frac{\partial \rho''}{\partial t} + \frac{\partial J_j{}''}{\partial x_j} = -\frac{\partial(\rho' u'_j)}{\partial x_j}, \tag{3.6c}$$

$$\frac{\partial}{\partial t}(\bar{\rho}q'' + \rho''\bar{q}) + \frac{\partial}{\partial x_j}(\bar{J}_j q'' + J''_j \bar{q}) = R''_q - \frac{\partial(\rho' q'_j)}{\partial t} - \frac{\partial}{\partial x_j}(\rho' u'_j \bar{q} + J'_j q'), \tag{3.6d}$$

thus obtaining

$$\bar{\rho}\frac{\partial q''}{\partial t} + \bar{J}_j \frac{\partial q''}{\partial x_j} = R''_q - J''_j \frac{\partial \bar{q}}{\partial x_j} + \bar{\rho}N''_{B,q}, \tag{3.7}$$

where J_j'' and R_q'' stand, respectively, for the second-order convective flux component and the second-order right-hand-side operator,

$$J_j'' = \rho''\bar{u}_j + \bar{\rho}u_j'', \tag{3.8a}$$

$$R_q'' = R_q(\bar{q}, \bar{\rho}, \bar{u}_j \cdots ; q'', \rho'', u_j'' \cdots ; q'\rho', q'u_j', \rho'u_j' \cdots), \tag{3.8b}$$

and $N_{B,q}''$ accounts for the 'bulk' interactions of first-order disturbances driven by base flow gradients,

$$N_{B,q}'' = -\frac{\rho'}{\bar{\rho}}\frac{\partial q'}{\partial t} - \frac{J_j'}{\bar{\rho}}\frac{\partial q'}{\partial x_j} - \frac{\rho'}{\bar{\rho}}u_j'\frac{\partial \bar{q}}{\partial x_j}. \tag{3.9}$$

In order to derive a form-invariant formulation of the problem, the right-hand-side second-order term R_q'' is recast as

$$R_q'' = R_{q''} + N_{S,q}'', \tag{3.10}$$

where $R_{q''}$ is only a function of the base flow properties and of the second-order disturbances, and has the same form as R_q':

$$R_{q''} = R_q(\bar{q}, \bar{\rho}, \bar{u}_j \cdots ; q'', \rho'', u_j'' \cdots). \tag{3.11}$$

Substituting (3.10) into (3.7) gives

$$\bar{\rho}\frac{\partial q''}{\partial t} + \bar{J}_j\frac{\partial q''}{\partial x_j} = R_{q''} - J_j''\frac{\partial \bar{q}}{\partial x_j} + N_{B,q}'' + N_{S,q}''. \tag{3.12}$$

For the velocity perturbations, $N_{S,u_i}'' = 0$, whereas for the temperature perturbations, $N_{S,T}''$ represents an additional contribution due to viscous effects and thermal power dissipation (whose expression is given in the next section).

3.3. *Disturbance governing equations*

From the above analysis, the conservation equations for the nth-order disturbances are then cast in the following form-invariant expression:

$$\frac{\partial \rho^{(n)}}{\partial t} + \bar{u}_j\frac{\partial \rho^{(n)}}{\partial x_j} + \bar{\rho}\frac{\partial u_j^{(n)}}{\partial x_j} + u_j^{(n)}\frac{\partial \bar{\rho}}{\partial x_j} + \rho^{(n)}\frac{\partial \bar{u}_j}{\partial x_j} = (n-1)N_{B,\rho}^{(n)}, \tag{3.13a}$$

$$\frac{\partial u_i^{(n)}}{\partial t} + \bar{u}_j\frac{\partial u_i^{(n)}}{\partial x_j} + \frac{1}{\bar{\rho}}\frac{\partial p^{(n)}}{\partial x_i} - \bar{\nu}\frac{\partial}{\partial x_j}\left(2S_{ij}^{(n)} - \frac{2}{3}S_{\ell\ell}^{(n)}\delta_{ij}\right) - \frac{1}{\bar{\rho}}\left(2S_{ij}^{(n)} - \frac{2}{3}S_{\ell\ell}^{(n)}\delta_{ij}\right)\frac{\partial \bar{\mu}}{\partial x_j} + \frac{1}{\bar{\rho}}(\rho^{(n)}\bar{u}_j + \bar{\rho}u_j^{(n)})\frac{\partial \bar{u}_i}{\partial x_j} = (n-1)N_{B,u_i}^{(n)}, \tag{3.13b}$$

$$\frac{\partial T^{(n)}}{\partial t} + \bar{u}_j\frac{\partial T^{(n)}}{\partial x_j} + \frac{1}{c_v}(p\theta)_L^{(n)} - \frac{1}{\bar{\rho}}\frac{\gamma}{Pr}\frac{\partial}{\partial x_j}\left(\bar{\mu}\frac{\partial T^{(n)}}{\partial x_j}\right) - \frac{1}{c_v}\phi_L^{(n)} + \frac{1}{\bar{\rho}}(\rho^{(n)}\bar{u}_j + \bar{\rho}u_j^{(n)})\frac{\partial \bar{T}}{\partial x_j} = (n-1)N_{B,T}^{(n)} + (n-1)N_{S,T}^{(n)}, \tag{3.13c}$$

$$p^{(n)} = R(\rho^{(n)}\bar{T} + \bar{\rho}T^{(n)}) + (n-1)N_{B,p}^{(n)}, \tag{3.13d}$$

where $n = 1, 2$ and $(\cdot)^{(n)}$ is here used to indicate the nth-order perturbation of any variable $(\cdot)$, and

$$(p\theta)_L^{(n)} = \left(p^{(n)}\frac{\partial \bar{u}_i}{\partial x_i} + \bar{p}\frac{\partial u_i^{(n)}}{\partial x_i}\right) \quad \text{and} \quad \phi_L^{(n)} = \bar{\nu}\left(4\bar{S}_{ij}S_{ij}^{(n)} - \frac{4}{3}\bar{S}_{\ell\ell}S_{kk}^{(n)}\right) \tag{3.14a,b}$$

are the nth-order linearized pressure–dilatation and the linearized viscous dissipation. In the sections that follow we use $N_q^{(n)} = N_{B,q}^{(n)} + N_{S,q}^{(n)}$. For $n = 1$, $N_{B,\rho}^{(1)} = 0$, $N_{B,u_i}^{(1)} = 0$, $N_{B,T}^{(1)} = 0$ and $N_{B,p}^{(1)} = 0$. For $n = 2$,

$$N_{B,\rho}^{(2)} = -\frac{\partial \rho^{(1)} u_j^{(1)}}{\partial x_j}, \tag{3.15a}$$

$$N_{B,u_i}^{(2)} = -\frac{\rho^{(1)}}{\bar{\rho}}\frac{\partial u_i^{(1)}}{\partial t} - \frac{1}{\bar{\rho}}(\rho^{(1)}\bar{u}_j + \bar{\rho}u_j^{(1)})\frac{\partial u_i^{(1)}}{\partial x_j} - \frac{\rho^{(1)}}{\bar{\rho}}u_j^{(1)}\frac{\partial \bar{u}_i}{\partial x_j}, \tag{3.15b}$$

$$N_{B,T}^{(2)} = -\frac{\rho^{(1)}}{\bar{\rho}}\frac{\partial T^{(1)}}{\partial t} - \frac{1}{\bar{\rho}}(\rho^{(1)}\bar{u}_j + \bar{\rho}u_j^{(1)})\frac{\partial T^{(1)}}{\partial x_j} - \frac{\rho^{(1)}}{\bar{\rho}}u_j^{(1)}\frac{\partial \bar{T}}{\partial x_j}, \tag{3.15c}$$

$$N_{B,p}^{(2)} = R\rho^{(1)}T^{(1)}, \tag{3.15d}$$

$$N_{S,T}^{(2)} = -\frac{1}{\bar{\rho}c_v}p^{(1)}\frac{\partial u_j^{(1)}}{\partial x_j} + \frac{\bar{\nu}}{c_v}\left(2S_{ij}^{(1)}S_{ij}^{(1)} - \frac{2}{3}S_{\ell\ell}^{(1)}S_{kk}^{(1)}\right). \tag{3.15e}$$

The governing equations for first- and second-order disturbances in Cartesian coordinates are given in supplementary material available at https://doi.org/10.1017/jfm.2024.912.

4. Stability analysis to second order

To account for the interactions between disturbances in the early phase of their evolution, the above equations are solved for both the first- and second-order disturbances.

In a compact form, the transport equations of the first-order disturbances (3.13*a*)–(3.13*d*) are cast in the form

$$\mathscr{L}(x, y, z, t; \bar{\rho}, \bar{u}, \ldots; \rho', u', v', w', p', T') = 0, \tag{4.1}$$

where $\mathscr{L}$ is the linearized compressible Navier–Stokes equations for the first-order disturbances and that has been derived in the previous section.

First-order disturbances are obtained by solving (4.1) for two-dimensional normal-form disturbances, yielding a generalized eigenvalue problem, whose solution gives a set of linearly independent eigenmodes $\hat{\boldsymbol{q}}'(y)$ (hereafter also referred to as modes) and the complex streamwise wavenumber α for a given angular frequency ω. The stability equations are solved in dimensionless form, where variables are made non-dimensional with respect to the free-stream values $(\rho_\infty, u_\infty, \rho_\infty u_\infty^2, T_\infty)$ and the Blasius length ℓ is used as reference length scale such that

$$Re = \frac{\rho_\infty u_\infty \ell}{\mu_\infty} = \sqrt{\frac{\rho_\infty u_\infty x}{\mu_\infty}} = \sqrt{Re_x}. \tag{4.2}$$

The non-dimensional frequencies are then given as

$$\omega = \frac{\omega^* \ell}{u_\infty} \quad \text{and} \quad F = \frac{\omega^* \mu_\infty}{\rho_\infty {u_\infty}^2}, \tag{4.3a,b}$$

where $\omega = ReF$ is the non-dimensional circular frequency.

For the transport equations of the second-order disturbances, we exploit the form-invariance form of (3.13*a*)–(3.13*d*) that are cast in the following compact form:

$$\mathscr{L}(x, y, z, t; \bar{\rho}, \bar{u}, \ldots; \rho'', u'', v'', w'', p'', T'') = \mathscr{N}(\bar{\rho}, \bar{u}, \ldots; \rho' u', \rho' v', \ldots), \tag{4.4}$$

where $\mathscr{N} = [N_{B,\rho}, N_{B,u_i}, N_{B,T} + N_{S,T}]$ represents the (weakly) nonlinear terms that drive the evolution of the second-order modes, which are assumed to have the normal form

$$\boldsymbol{q}'' = \hat{\boldsymbol{q}}''(y) \exp\left(\mathrm{i}\left(\int^x \alpha \, \mathrm{d}x - \omega t\right)\right). \tag{4.5}$$

Introducing the normal-mode expansion of the disturbances, a single set of equations is written for the first- and second-order modes ($\hat{\boldsymbol{q}}'$ and $\hat{\boldsymbol{q}}''$). Assuming a two-dimensional non-parallel flow with the base flow assumed to vary in both the streamwise and wall-normal directions, namely $\bar{u} = \bar{u}(x, y)$, $\bar{v} = \bar{v}(x, y)$, $\bar{w} = 0$, $\bar{\rho} = \bar{\rho}(x, y)$, $\bar{T} = \bar{T}(x, y)$, $\bar{p} = \bar{p}(x, y)$, the stability equations for the first- and second-order modes are recovered. In a compact matrix form, the stability equations are cast as

$$\boldsymbol{C}\frac{\mathrm{d}^2 \hat{\boldsymbol{q}}}{\mathrm{d}y^2} + \boldsymbol{B}\frac{\mathrm{d}\hat{\boldsymbol{q}}}{\mathrm{d}y} + \boldsymbol{A}\hat{\boldsymbol{q}} = (n-1) f \hat{\boldsymbol{N}}, \tag{4.6}$$

where $\boldsymbol{A} = \boldsymbol{A}(\alpha, \omega, M, Re; \bar{\rho}, \bar{u}_i, \bar{p}, \bar{T})$, $\boldsymbol{B} = \boldsymbol{B}(\alpha, \omega, M, Re; \bar{\rho}, \bar{u}_i, \bar{p}, \bar{T})$ and $\boldsymbol{C} = \boldsymbol{C}(\alpha, \omega, M, Re; \bar{\rho}, \bar{u}_i, \bar{p}, \bar{T})$ are (5×5) matrices whose expressions are given in Appendix B; $\hat{\boldsymbol{N}}$ is the normal-mode representation of the first-order mode interaction contribution to the second-order ones. The density mode and its x and y derivatives are determined from the linearized equation of state. Note that the viscosity disturbances $((\mathrm{d}\bar{\mu}/\mathrm{d}T)\hat{T}'$ and $(\mathrm{d}\bar{\mu}/\mathrm{d}T)\hat{T}''$, respectively) have been found not to affect the stability (for brevity, results of the analysis are not reported) and have been neglected. The factor $f = \exp(\mathrm{i}(\int^x \alpha \, \mathrm{d}x - \omega_0 T_0/2)) \sin(\omega_0 T_0/2)/(\omega_0 T_0/2)$ accounts for cycle-averaged nonlinear effects (Kuehl 2018), where ω_0 and T_0 are, respectively, the angular frequency and the corresponding period at synchronization location $T_0 = \ell_0/u_\infty$ (ℓ_0 being the Blasius length at synchronization). In practice, a first LST calculation is performed to determine the synchronization frequency corresponding to the maximum amplification of the unstable mode, which provides the reference Blasius length ℓ_0 to form the reference Reynolds number Re_0 for LST computations. In the following, the results are presented using the local Reynolds number Re and the dimensionless phase speed $c_\varphi = \omega/\alpha = c_r + ic_i$ is used, as suggested by Lifshitz *et al.* (2012), since its value does not depend on the length scale ℓ_0 (contrary to the complex wavenumber that does depend on ℓ_0). To account for the thickening of the boundary layer, the base flow equations are solved in the transformed space $(x, y/\delta(x))$, and ℓ_0 and the corresponding Reynolds number Re_0 are chosen as reference.

For $n = 1$, (B1) reduces to the linear stability equation

$$\hat{\boldsymbol{L}}\hat{\boldsymbol{q}}' = 0, \tag{4.7}$$

where

$$\hat{\boldsymbol{L}} = \boldsymbol{C}\frac{\mathrm{d}^2}{\mathrm{d}y^2} + \boldsymbol{B}\frac{\mathrm{d}}{\mathrm{d}y} + \boldsymbol{A} = \hat{\boldsymbol{L}}(\alpha, \omega, M, Re; \bar{\rho}, \bar{u}_i, \bar{p}, \bar{T}), \tag{4.8}$$

with homogeneous boundary conditions. Namely, $\hat{u}' = \hat{v}' = \hat{w}' = 0$ and $\mathrm{d}\hat{p}'/\mathrm{d}y = 0$, both at the wall and at free stream, and $\hat{T}' = 0$ at the wall and $\mathrm{d}\hat{T}'/\mathrm{d}y = 0$ at free stream.

Equation (4.7) constitutes an eigenvalue problem in the wavenumber α that depends on the Mach and Reynolds numbers. The discretized eigenproblem is transformed into a problem with linear eigenvalues, and solved with the shift-invert method and a QZ algorithm and taking $\bar{v} = 0$. A Newton–Raphson algorithm is implemented to follow the selected modes (see Gloerfelt & Robinet (2017) for more details).

For $n = 2$, the second-order stability equation is

$$\hat{\boldsymbol{L}}\hat{\boldsymbol{q}}'' = f\hat{\boldsymbol{N}}. \tag{4.9}$$

The second-order modes are then computed from the relation

$$\hat{\boldsymbol{q}}'' = f\hat{\boldsymbol{L}}^{-1}\hat{\boldsymbol{N}}. \tag{4.10}$$

To second order, the disturbance mode of any variable q is then computed as the sum of the first- and second-order modes ($\epsilon\hat{\boldsymbol{q}}' + \epsilon^2\hat{\boldsymbol{q}}''$).

4.1. *Linear stability results*

The influence of the Mach number and of the wall thermal state is here analysed considering both adiabatic and cold-wall conditions (see table 1). In the table we also report the values of the Mach numbers and the corresponding values of the boundary-layer thickness (δ_0), the generalized inflection point distance (y_{gip}), the sonic line y position ($y_{s,S}$ and $y_{s,F}$ of the slow and fast modes, respectively) and the critical layer height ($y_{c,S}$ and $y_{c,F}$) at synchronization location (i.e. at the reference streamwise location), where y_{gip} is defined as $\partial/\partial y(\bar{\rho}\partial\bar{u}/\partial y) = 0$. The selected conditions of the adiabatic wall cases are those of Ma & Zhong (2003*a*) and Reed & Balakumar (1990) for $M = 4.5$ and $M = 6$, respectively, whereas for the cold-wall cases they are those of Fedorov & Tumin (2011). For the former, the selected non-dimensional frequency is $F = 2.2 \times 10^{-4}$; for the cold-wall cases the selected value of F is 1×10^{-4}. All selected cases are inviscidly unstable. As expected, the generalized inflection point moves farther away from the wall as the Mach number increases, with the exception of the $M = 5.5$ case that presents an inflection point at the wall.

For comparison with the literature, all results are presented in terms of the local Reynolds number (4.2), the growth rate being represented in terms of the imaginary part of the phase speed c_i (Lifshitz *et al.* 2012). Figure 1 showcases the real and imaginary parts of the phase speeds that are in very good agreement with the literature (symbols in figure 1). Note that the vertical dashed lines in the figure identify the analysed domain around synchronization location. The slow mode of the adiabatic ($M = 4.5$ and $M = 6$) and cold ($M = 6.5$) wall cases is initially unstable, whereas for $M = 5.5$ the fast mode is initially unstable. The unstable mode (slow or fast) reaches its maximum amplification as the other mode (fast or slow) attains a minimum. The phase velocity of the two modes

M	T_∞ (K)	p_∞ (N m^{-2})	T_{wall} (K)	δ_0	y_{gip}	$y_{s,S}$	$y_{s,F}$	$y_{c,S}$	$y_{c,F}$
4.5	65.15	728.4	T_{ad}	16.0	11.2	5.8	5.8	11.5	11.2
6	65	2421.8	T_{ad}	21.8	17.3	9.7	9.7	17.3	17.3
5.5	70	2421.4	$6.1T_\infty/10$	10	0	3.6	3.4	6.0	5.8
6.5	70	2421.4	$8.1T_\infty/10$	11.5	19.2	10.6	10.6	18.7	18.7

Table 1. Base flow boundary-layer parameters (thickness, generalized inflection point, sonic line and critical layer heights) for various Mach numbers.

is then very close, and this phenomenon is called synchronization. Past synchronization location, mode S of the two adiabatic cases and of the cold case at $M = 5.5$ exhibits a slightly increasing Mach number (relative to the phase speed) still remaining subsonic, whereas mode F shows a continuously decreasing phase speed. An opposite behaviour is observed for case $M = 6.5$, namely the phase speed of the fast mode has a tendency to increase whereas it continuously decreases for mode S.

The wall-normal distributions of the eigenfunction amplitudes and phases at synchronization location are reported in figure 2 for the slow and the fast modes, respectively. The amplitudes are normalized by the pressure amplitude at the wall. The behaviour of the adiabatic (respectively, cold) wall cases being similar, unless significant differences occur, hereafter we only report the results for $M = 4.5$ and $M = 5.5$. The figure shows that the eigenfunctions are dominated by the fluctuations in thermodynamic variables. In the subsonic layer, pressure, temperature and streamwise velocity perturbations are approximately in phase and in nearly phase opposition with the wall-normal velocity. It is also interesting to observe that for the cold wall the reduction of the boundary-layer scales affects the initially unstable mode that experiences a smaller peak in the temperature perturbation amplitude at the critical layer. The phase behaviour is overall less affected by the wall thermal conditions.

4.2. *Budget analysis*

To identify the dominant physical mechanisms and to elucidate their role in the slow and fast modes, we have scrutinized the budgets of the various perturbation variables at synchronization location. In the following, we report the budgets of the streamwise and wall-normal velocity and temperature disturbances that are discussed in detail in the discussion section.

For the analysis, the total time rate of change of any variable $\widehat{(\cdot)}$ is split in two terms, namely $(\hat{\mathrm{D}}/\mathrm{D}t)\widehat{(\cdot)} = \mathrm{i}(\alpha\bar{u} - \omega)\widehat{(\cdot)}$ (which accounts for the streamwise contribution) and $\bar{v}(d\widehat{(\cdot)}/\mathrm{d}y)$ that represents the (convective) transport due to base flow wall-normal velocity component.

Dropping superscripts $\hat{(\cdot)}'$ and $\hat{(\cdot)}''$, the normal-mode expression of the budget equation for the streamwise velocity disturbance (of either first or second order) is cast in the form

$$\frac{\hat{\mathrm{D}}\hat{u}}{\mathrm{D}t} + \bar{v}\frac{\mathrm{d}\hat{u}}{\mathrm{d}y} = -\mathrm{i}\alpha\frac{\hat{p}}{\bar{\rho}} + D_u + u\text{-}mgP + (n-1)f\hat{N}_u, \tag{4.11}$$

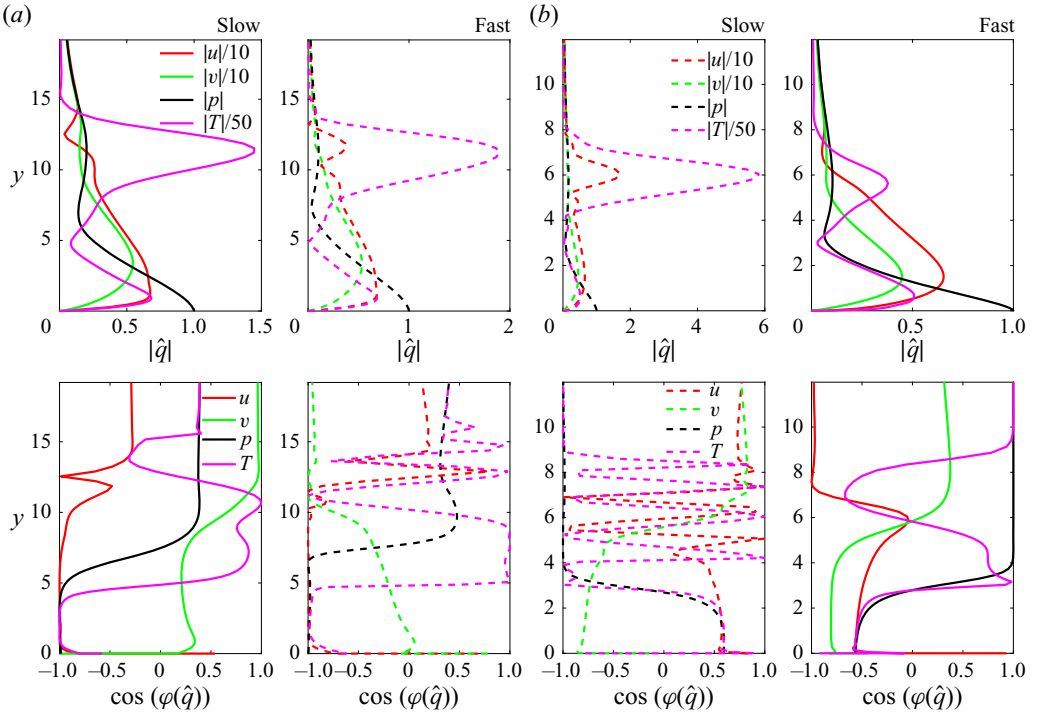

Figure 2. Eigenfunction amplitudes and phases at synchronization location for (*a*) adiabatic wall ($M = 4.5$) and (*b*) cold wall ($M = 5.5$). Solid lines, initially unstable mode; dashed lines, initially stable mode.

where

$$\frac{\hat{\mathrm{D}}\hat{u}}{\mathrm{D}t} = \mathrm{i}\left(\alpha\bar{u} - \omega\right)\hat{u}, \tag{4.12a}$$

$$D_u = \frac{1}{\bar{\rho}}\left\{\left[\frac{4}{3}\bar{\mu}\left(\mathrm{i}\frac{\mathrm{d}\alpha}{\mathrm{d}x} - \alpha^2\right) + \frac{4}{3}\mathrm{i}\alpha\frac{\partial\bar{\mu}}{\partial y}\right]\hat{u} + \bar{\mu}\frac{\mathrm{d}^2\hat{u}}{\mathrm{d}y^2} + \frac{\partial\bar{\mu}}{\partial y}\frac{\mathrm{d}\hat{u}}{\mathrm{d}y} + \mathrm{i}\alpha\frac{\partial\bar{\mu}}{\partial y}\hat{v} + \left(\mathrm{i}\frac{1}{3}\alpha\bar{\mu} - \frac{2}{3}\frac{\partial\bar{\mu}}{\partial x}\right)\frac{\mathrm{d}\hat{v}}{\mathrm{d}y}\right\}, \tag{4.12b}$$

$$u\text{-}mgP = -\left[\hat{u} + \bar{u}\left(\frac{\hat{p}}{\bar{p}} - \frac{\hat{T}}{\bar{T}}\right)\right]\frac{\partial\bar{u}}{\partial x} - \left[\hat{v} + \bar{v}\left(\frac{\hat{p}}{\bar{p}} - \frac{\hat{T}}{\bar{T}}\right)\right]\frac{\partial\bar{u}}{\partial y}, \tag{4.12c}$$

$$\hat{N}_u = \frac{1}{\bar{\rho}}\left[\mathrm{i}\omega\hat{\rho}'\hat{u}' - \mathrm{i}\alpha(\hat{\rho}'\bar{u} + \bar{\rho}\hat{u}')\hat{u}' - (\hat{\rho}'\bar{v} + \bar{\rho}\hat{v}')\frac{\mathrm{d}\hat{u}'}{\mathrm{d}y} - \hat{\rho}'\hat{u}'\frac{\partial\bar{u}}{\partial x} - \hat{\rho}'\hat{v}'\frac{\partial\bar{u}}{\partial y}\right], \tag{4.12d}$$

where $n = 1$ for the budget of the first-order mode $(\hat{\cdot})'$ and $n = 2$ for the second-order mode $(\hat{\cdot})''$. The right-hand side of (4.11) represents the contributions due to the streamwise pressure gradient, diffusion, transport of streamwise momentum disturbances resulting from the base flow/perturbation interaction driven by the base flow velocity gradient and the contribution resulting from the interaction of first-order modes.

The budget equation for the wall-normal velocity disturbance is written as

$$\frac{\hat{\mathrm{D}}\hat{v}}{\mathrm{D}t} + \bar{v}\frac{\mathrm{d}\hat{v}}{\mathrm{d}y} = -\frac{1}{\bar{\rho}}\frac{\mathrm{d}\hat{p}}{\mathrm{d}y} + D_v + v\text{-}mgP + (n-1)f\hat{N}_v, \tag{4.13}$$

with $n = 1, 2$, and where

$$\frac{\hat{\mathrm{D}}\hat{v}}{\mathrm{D}t} = \mathrm{i}(\alpha\bar{u} - \omega)\hat{v}, \tag{4.14a}$$

$$\begin{aligned} D_v = \frac{1}{\bar{\rho}}\Bigg\{ & -\frac{2}{3}\mathrm{i}\alpha\frac{\partial\bar{\mu}}{\partial y}\hat{u} + \left(\mathrm{i}\frac{1}{3}\alpha\bar{\mu} - \frac{\partial\bar{\mu}}{\partial x}\right)\frac{\mathrm{d}\hat{u}}{\mathrm{d}y} \\ & \times \left[\bar{\mu}\left(\mathrm{i}\frac{\mathrm{d}\alpha}{\mathrm{d}x} - \alpha^2\right) + \mathrm{i}\alpha\frac{\partial\bar{\mu}}{\partial x}\right]\hat{v} + \frac{4}{3}\left(\bar{\mu}\frac{\mathrm{d}^2\hat{v}}{\mathrm{d}y^2} + \frac{\partial\bar{\mu}}{\partial y}\frac{\mathrm{d}\hat{v}}{\mathrm{d}y}\right)\Bigg\}, \end{aligned} \tag{4.14b}$$

$$v\text{-}mgP = -\left[\hat{u} + \bar{u}\left(\frac{\hat{p}}{\bar{p}} - \frac{\hat{T}}{\bar{T}}\right)\right]\frac{\partial\bar{v}}{\partial x} - \left[\hat{v} + \bar{v}\left(\frac{\hat{p}}{\bar{p}} - \frac{\hat{T}}{\bar{T}}\right)\right]\frac{\partial\bar{v}}{\partial y}, \tag{4.14c}$$

$$\hat{N}_v = \frac{1}{\bar{\rho}}\left[\mathrm{i}\omega\hat{\rho}'\hat{v}' - \mathrm{i}\alpha(\hat{\rho}'\bar{u} + \bar{\rho}\hat{u}')\hat{v}' - \left(\hat{\rho}'\bar{v} + \bar{\rho}\hat{v}'\right)\frac{\mathrm{d}\hat{v}'}{\mathrm{d}y} - \hat{\rho}'\hat{u}'\frac{\partial\bar{v}}{\partial x} - \hat{\rho}'\hat{v}'\frac{\partial\bar{v}}{\partial y}\right]. \tag{4.14d}$$

Similarly, the budget equation for the temperature disturbance $\hat{T} = \hat{e}/c_v$ is written as

$$\frac{\hat{\mathrm{D}}\hat{T}}{\mathrm{D}t} + \bar{v}\frac{\mathrm{d}\hat{T}}{\mathrm{d}y} = -\frac{1}{\bar{\rho}c_v}(p\theta)_L + D_T + \frac{1}{c_v}\hat{\phi}_L + T\text{-}mgP + (n-1)f\hat{N}_T \tag{4.15}$$

($n = 1, 2$), where $\hat{\mathrm{D}}\hat{T}/\mathrm{D}t$, $(p\theta)_L$, D_T, $\hat{\phi}_L$, $\hat{\phi}_{T,L}$, $T\text{-}mgP$ and $\hat{N}_T$ stand for, respectively, the total time rate of change of $\hat{T}$, the exchanges of internal energy due to (linearized) pressure–dilatation and heat conduction, the (linearized) viscous dissipation contribution, the (linearized) thermal power dissipation, the exchanges of internal energy disturbances resulting from base flow/perturbation interaction driven by base flow temperature gradients and the contribution resulting from first-order mode interactions, whose expressions are given in the following:

$$\frac{\hat{\mathrm{D}}\hat{T}}{\mathrm{D}t} = \mathrm{i}(\alpha\bar{u} - \omega)\hat{T}, \tag{4.16a}$$

$$(p\theta)_L = -\bar{p}\left(\mathrm{i}\alpha\hat{u} + \frac{\mathrm{d}\hat{v}}{\mathrm{d}y}\right) - \hat{p}\left(\frac{\partial\bar{u}}{\partial x} + \frac{\partial\bar{v}}{\partial y}\right), \tag{4.16b}$$

$$D_T = \frac{\gamma}{Pr}\frac{1}{\bar{\rho}}\left\{\left[\bar{\mu}\left(-\alpha^2 + \mathrm{i}\frac{\mathrm{d}\alpha}{\mathrm{d}x}\right) + \mathrm{i}\alpha\frac{\partial\bar{\mu}}{\partial x}\right]\hat{T} + \left[\bar{\mu}\frac{\mathrm{d}^2\hat{T}}{\mathrm{d}y^2} + \frac{\partial\bar{\mu}}{\partial y}\frac{\mathrm{d}\hat{T}}{\mathrm{d}y}\right]\right\}, \tag{4.16c}$$

$$\hat{\phi}_L = \bar{\nu}\left\{4\left(\frac{\partial\bar{u}}{\partial x}\mathrm{i}\alpha\hat{u} + \frac{\partial\bar{v}}{\partial y}\frac{\mathrm{d}\hat{v}}{\mathrm{d}y}\right) + 2\left(\frac{\partial\bar{u}}{\partial y} + \frac{\partial\bar{v}}{\partial x}\right)\left(\frac{\mathrm{d}\hat{u}}{\mathrm{d}y} + \mathrm{i}\alpha\hat{v}\right)\right.$$
$$\left. -\frac{4}{3}\left(\frac{\partial\bar{u}}{\partial x} + \frac{\partial\bar{v}}{\partial y}\right)\left(\mathrm{i}\alpha\hat{u} + \frac{\mathrm{d}\hat{v}}{\mathrm{d}y}\right)\right\}, \tag{4.16d}$$

$$T\text{-}mgP = -\left[\hat{u} + \bar{u}\left(\frac{\hat{p}}{\bar{p}} - \frac{\hat{T}}{\bar{T}}\right)\right]\frac{\partial\bar{T}}{\partial x} - \left[\hat{v} + \bar{v}\left(\frac{\hat{p}}{\bar{p}} - \frac{\hat{T}}{\bar{T}}\right)\right]\frac{\partial\bar{T}}{\partial y}, \tag{4.16e}$$

$$\hat{N}_T = \frac{1}{\bar{\rho}}\left\{\mathrm{i}\omega\hat{\rho}'\hat{T}' - \mathrm{i}a(\hat{\rho}'\bar{u} + \bar{\rho}\hat{u}')\hat{T}' - (\hat{\rho}'\bar{v} + \bar{\rho}\hat{v}')\frac{\mathrm{d}\hat{T}}{\mathrm{d}y} - \hat{\rho}'\hat{u}'\frac{\partial\bar{T}}{\partial x} - \hat{\rho}'\hat{v}'\frac{\partial\bar{T}}{\partial y}\right.$$
$$-\frac{1}{c_v}\hat{p}'\left(\mathrm{i}\alpha\hat{u}' + \frac{\mathrm{d}\hat{v}'}{\mathrm{d}y}\right) + \frac{\bar{\mu}}{c_v}\left[-2\alpha^2(\hat{u}')^2 + 2\left(\frac{\mathrm{d}\hat{v}'}{\mathrm{d}y}\right)^2 + \left(\frac{\mathrm{d}\hat{u}'}{\mathrm{d}y} + \mathrm{i}\alpha\hat{v}'\right)^2\right.$$
$$\left.\left. -\alpha^2(\hat{w}')^2 + \left(\frac{\mathrm{d}\hat{w}'}{\mathrm{d}y}\right)^2 - \frac{2}{3}\left(\mathrm{i}\alpha\hat{u}' + \frac{\mathrm{d}\hat{v}'}{\mathrm{d}y}\right)^2\right] + \left(\bar{u}\frac{\partial\bar{T}}{\partial x} + \bar{v}\frac{\partial\bar{T}}{\partial y}\right)\hat{\rho}'\frac{\hat{T}'}{\bar{T}}\right\}. \tag{4.16f}$$

To interpret and understand the physical mechanisms controlling the wall behaviour of the perturbations we have also analysed in detail the budgets in the near-wall proximity (i.e. in the limit $y \to 0$). Taking into account the boundary conditions at the wall, namely $\hat{u} = \hat{v} = \hat{w} = \hat{T} = 0$ and $\bar{u} = \bar{v} = \partial\bar{p}/\partial y = 0$, the normal-mode expression of the continuity equation (3.13*a*) and equations (4.11), (4.13) and (4.15) reduce to

$$\frac{\mathrm{d}\hat{v}}{\mathrm{d}y} = \mathrm{i}\omega\frac{\hat{p}}{\bar{p}} - \frac{\partial\bar{v}}{\partial y}\frac{\hat{p}}{\bar{p}} - (n-1)f\frac{\hat{p}'}{\bar{p}}\frac{\mathrm{d}\hat{v}'}{\mathrm{d}y}, \tag{4.17a}$$

$$\bar{\mu}\frac{\mathrm{d}^2\hat{u}}{\mathrm{d}y^2} = \mathrm{i}\alpha\hat{p} + \frac{2}{3}\frac{\mathrm{d}\hat{v}}{\mathrm{d}y}\frac{\partial\bar{\mu}}{\partial x} - \frac{\mathrm{d}\hat{u}}{\mathrm{d}y}\frac{\partial\bar{\mu}}{\partial y}, \tag{4.17b}$$

$$\frac{4}{3}\bar{\mu}\frac{\mathrm{d}^2\hat{v}}{\mathrm{d}y^2} = \frac{\mathrm{d}\hat{p}}{\mathrm{d}y} - \frac{4}{3}\frac{\mathrm{d}\hat{v}}{\mathrm{d}y}\frac{\partial\bar{\mu}}{\partial y} - \frac{\mathrm{d}\hat{u}}{\mathrm{d}y}\frac{\partial\bar{\mu}}{\partial x}, \tag{4.17c}$$

$$\bar{p}\frac{\mathrm{d}\hat{v}}{\mathrm{d}y} = \frac{c_p}{Pr}\frac{\mathrm{d}}{\mathrm{d}y}\left(\bar{\mu}\frac{\mathrm{d}\hat{T}}{\mathrm{d}y}\right) + \left[\frac{8}{3}\bar{\mu}\frac{\partial\bar{v}}{\partial y}\frac{\mathrm{d}\hat{v}}{\mathrm{d}y} + 2\bar{\mu}\frac{\partial\bar{u}}{\partial y}\frac{\mathrm{d}\hat{u}}{\mathrm{d}y}\right] - \hat{p}\frac{\partial\bar{v}}{\partial y}$$
$$-(n-1)f\left(\hat{p}'\frac{\mathrm{d}\hat{v}'}{\mathrm{d}y} - \bar{\rho}\hat{\phi}'\right), \tag{4.17d}$$

where $\hat{\phi}' = \bar{\nu}[\frac{4}{3}(\mathrm{d}\hat{v}'/\mathrm{d}y)^2 + (\mathrm{d}\hat{u}'/\mathrm{d}y)^2 + (\mathrm{d}\hat{w}'/\mathrm{d}y)^2]$ and $n = 1, 2$.

4.2.1. *The u budget*

Figure 3 reports the amplitudes and phases of the various terms of the budgets of the slow and fast $\hat{u}$ modes at synchronization location for adiabatic wall ($M = 4.5$) and cold wall ($M = 5.5$). At $M = 4.5$, $\hat{D}\hat{u}/\mathrm{D}t$ is primarily driven by the streamwise pressure gradient and by the base flow/perturbation interaction term. The latter attains a maximum in the subsonic layer (at $y/\delta \approx 1/4$), whereas $\hat{\mathrm{D}}\hat{u}/\mathrm{D}t$ is maximum in the very near-wall region ($y/\delta \approx 1/10$). The figure also shows that the effect of *u-mgP* is stronger for cold wall than for adiabatic wall. It is worth noting that this one-way coupling term reflects the

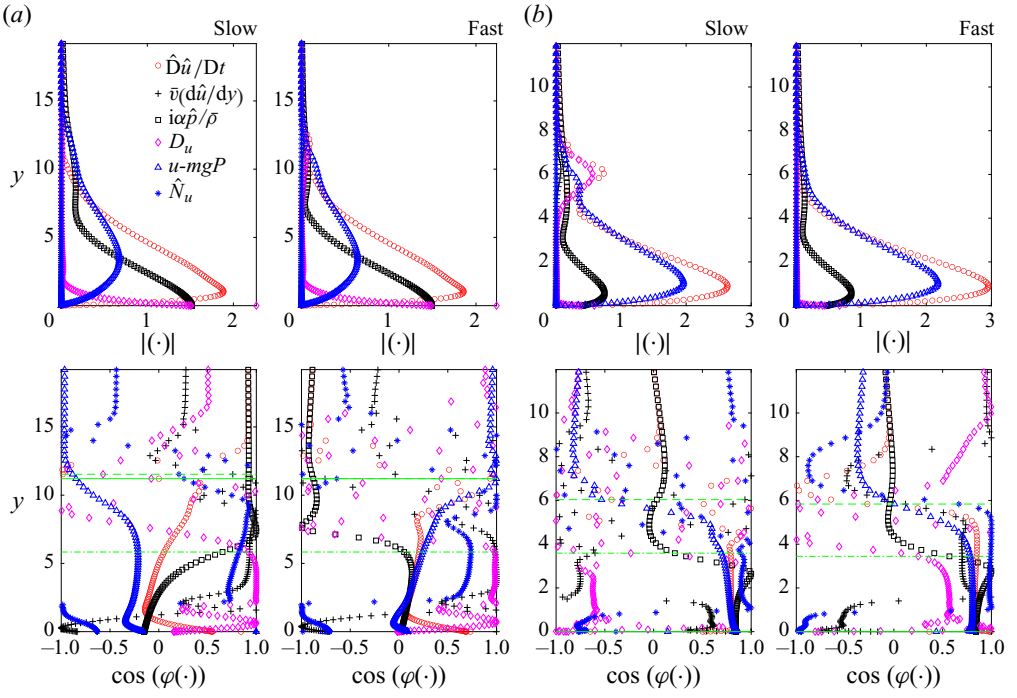

Figure 3. Budgets of the streamwise velocity perturbation of modes S and F for (*a*) adiabatic wall ($M = 4.5$) and (*b*) cold wall ($M = 5.5$). Modulus in the first row and phase in the second row.

assumption that the base flow and the disturbances are weakly coupled. Namely, the reciprocal effect leading to base flow distortion is neglected. At the wall, as predicted from the asymptotic perturbation equation (4.17*b*), diffusion and streamwise pressure gradient are in equilibrium (namely, diffusion of the perturbation streamwise velocity is dictated by the streamwise pressure gradient).

For fast modes, $\hat{\mathrm{D}}\hat{u}/\mathrm{D}t$, $-\mathrm{i}\alpha(1/\bar{\rho})\hat{p}$ and u-mgP are approximately in phase within the subsonic layer. For slow modes, $\hat{\mathrm{D}}\hat{u}/\mathrm{D}t$ and $-\mathrm{i}\alpha(1/\bar{\rho})\hat{p}$ are nearly in phase opposition in the vicinity of the critical layer (where $\bar{u} = c_r$). At the critical layer $\hat{\mathrm{D}}\hat{u}/\mathrm{D}t$ exhibits a phase jump. Note that no significant change in the behaviour is observed across synchronization (data not reported).

4.2.2. *The v budget*

The budgets of the slow and fast $\hat{v}$ modes are displayed in figure 4. The evolution of the wall-normal perturbation velocity mode $\hat{v}$ is essentially driven by the wall-normal pressure gradient. Its total time rate of change $\hat{\mathrm{D}}\hat{v}/\mathrm{D}t$ and $-(1/\bar{\rho})(\mathrm{d}\hat{p}/\mathrm{d}y)$ superpose in both amplitude and phase, for both slow and fast modes and for all Mach numbers. At the wall, as in the case of the perturbation streamwise velocity, diffusion balances the perturbation wall-normal pressure gradient.

The streamwise distributions of the amplitude and phase of the wall perturbation–dilatation $\theta = \mathrm{d}\hat{v}/\mathrm{d}y$, the (negative) time rate of change of the pressure perturbation $\mathrm{i}\omega(\hat{p}/\bar{p})$ and the (negative) mean dilatation term $-(\hat{p}/\bar{p})\bar{\theta}$ $(\bar{\theta} = \partial\bar{v}/\partial y)$ around synchronization are reported in figure 5 for both the S and F modes. The figure shows

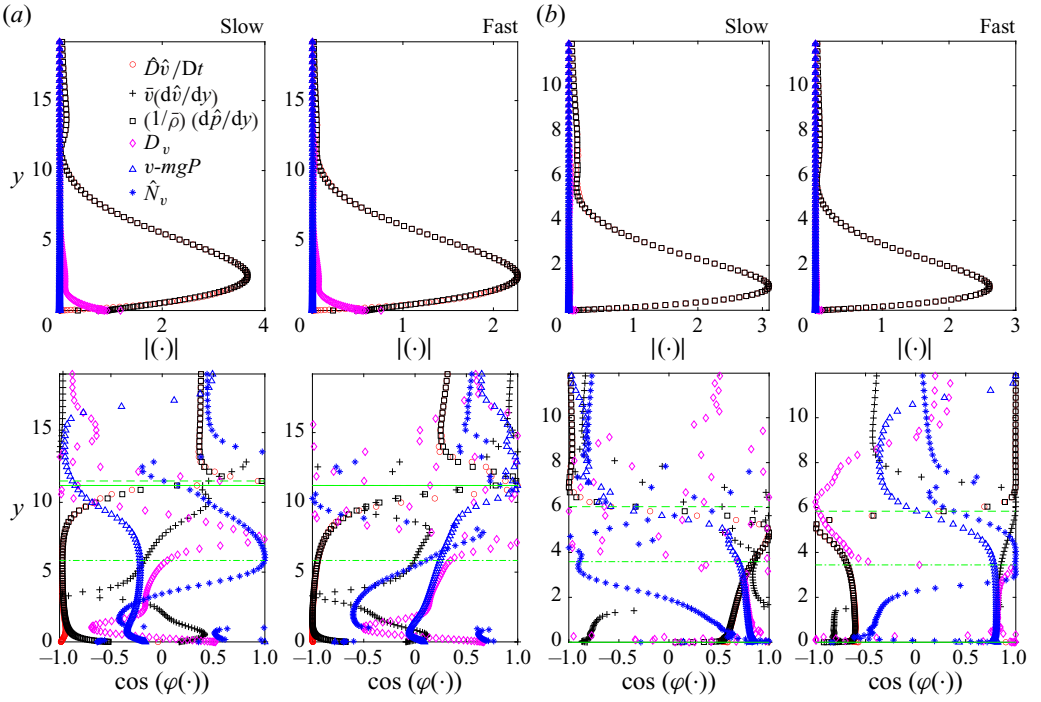

Figure 4. Budgets of the wall-normal velocity perturbation of modes S and F for (*a*) adiabatic wall ($M = 4.5$) and (*b*) cold wall ($M = 5.5$).

that, in the near-wall proximity, the effect of the mean dilatation is negligible and $\mathrm{d}\hat{v}/\mathrm{d}y \approx \mathrm{i}\omega(\hat{p}/\bar{p})$; namely, the wall perturbation–dilatation is driven by the time rate of change of pressure perturbation with a phase lag of approximately 90° independently of the Mach number.

4.2.3. *The T budget*

For adiabatic wall, the budgets of the slow and fast $\hat{T}$ modes (figure 6) show that, in the subsonic layer, $\hat{\mathrm{D}}\hat{T}/\mathrm{D}t$ is primarily driven by the (linearized) pressure–dilatation $(p\theta)_L$. In the supersonic region, in addition to heat conduction effects (whose contribution is most significant in the proximity of the critical layer), the exchanges of internal energy associated with the perturbation/base flow interaction (T-mgP) also play a role. For cold wall, in the subsonic layer $\hat{\mathrm{D}}\hat{T}/\mathrm{D}t$ is controlled by $(p\theta)_L$ and T-mgP. Dilatational effects are then expected to be strongly influenced by energy exchanges induced by base flow temperature gradients. It is also interesting to observe that near the critical layer the initially stable mode S is also controlled by pressure–dilatation effects in addition to heat conduction.

In the supersonic and subsonic (away from the wall) layers, $\hat{\mathrm{D}}\hat{T}/\mathrm{D}t$ and $-(p\theta)_L$ are approximately in phase at all Mach numbers. In agreement with (4.17*d*), figure 6 also shows that for all cases, near the wall, the perturbation pressure–dilatation approximately balances the heat conduction term $(\bar{p}(\mathrm{d}\hat{v}/\mathrm{d}y) \approx (c_p/Pr)(\mathrm{d}/\mathrm{d}y)(\bar{\mu}(\mathrm{d}\hat{T}/\mathrm{d}y)))$, since the mean dilatation and the linearized viscous dissipation are approximately negligible.

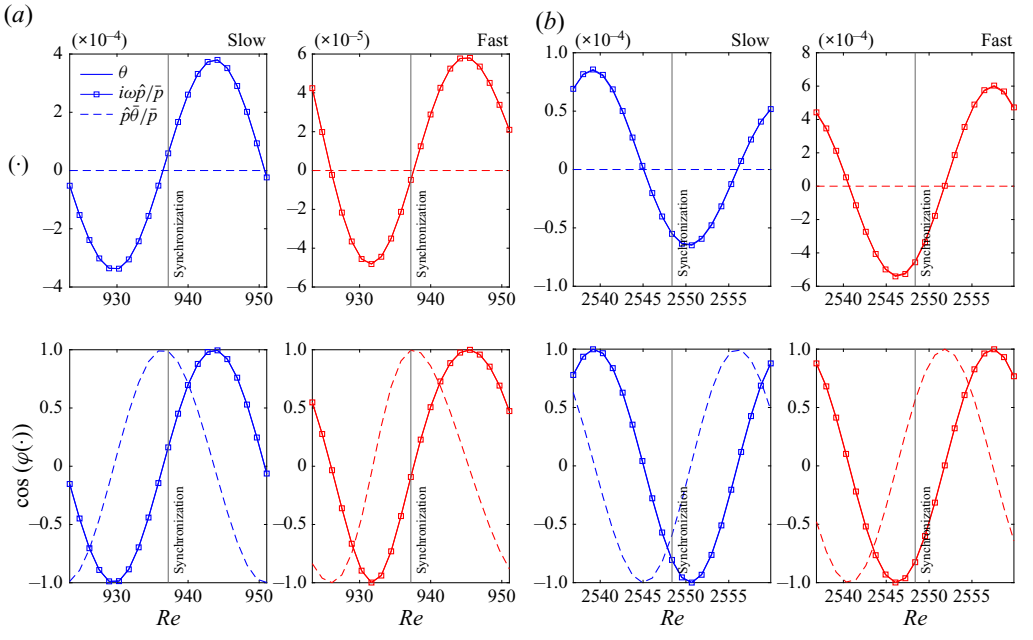

Figure 5. Streamwise distribution of wall dilatation of modes S and F for (*a*) adiabatic wall ($M = 4.5$) and (*b*) cold wall ($M = 5.5$). Upper panels, amplitude; lower panels, phase.

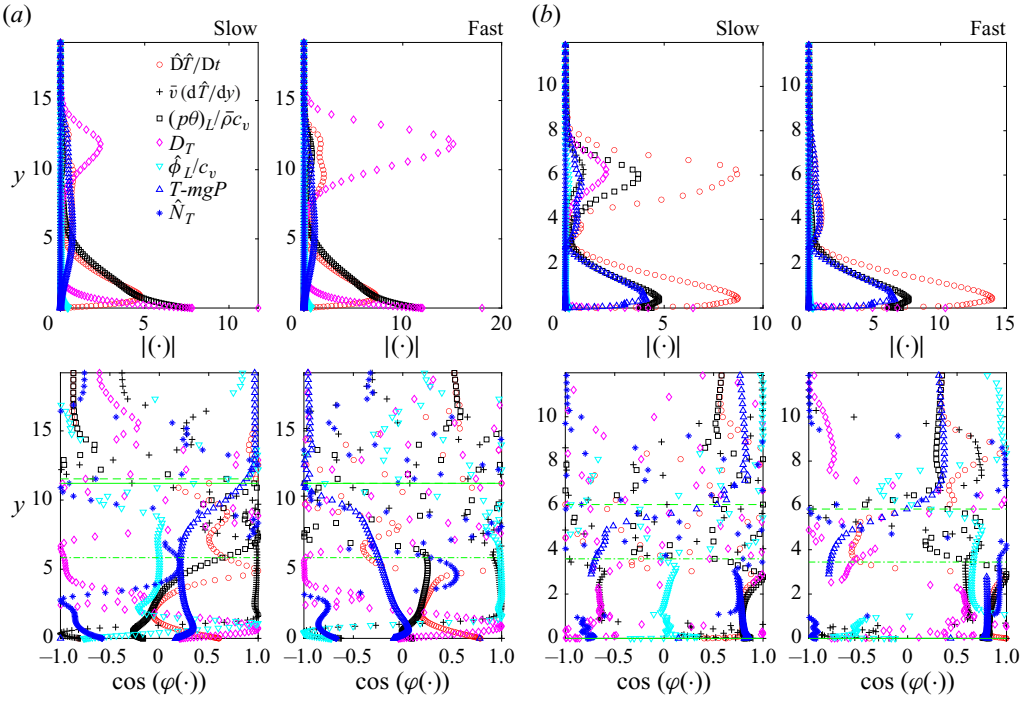

Figure 6. Budgets of the temperature perturbation of modes S and F for (*a*) adiabatic wall ($M = 4.5$) and (*b*) cold wall ($M = 5.5$).

The above results confirm those of Chen *et al.* (2023*a*) who conducted a comparative study on the dominant energy source terms showing that $\bar{p}\hat{\theta}$ plays a dominant role near the wall, whereas away from the wall mean temperature gradients play also a role in the energy redistribution through the perturbation/base flow interaction term *T-mgP*.

4.2.4. *Nonlinear interaction*

We assume that the interaction of a mode $\hat{\boldsymbol{q}}_{I_1}$ (where I_1 stands for either S or F) with a mode $\hat{\boldsymbol{q}}_{I_2}$ (I_2 standing for either F or S) produces a mode $\hat{\boldsymbol{q}}_{I_1} = \epsilon\hat{\boldsymbol{q}}'_{I_1} + \epsilon^2\hat{\boldsymbol{q}}''_{I_{1/2}}$, where the second-order mode is obtained from (4.10):

$$\hat{\boldsymbol{q}}''_{I_{1/2}} = f\hat{\boldsymbol{L}}^{-1}\hat{\boldsymbol{N}}_q^{I_1/I_2}, \tag{4.18}$$

with $\hat{\boldsymbol{N}}_q^{I_1/I_2} = \hat{\boldsymbol{N}}_q(\bar{\rho}, \bar{u}, \ldots; \hat{\rho}'_{I_1}\hat{u}'_{I_2}, \hat{\rho}'_{I_1}\hat{v}'_{I_2}, \ldots)$ representing the nonlinear contribution due to cross-interactions.

For self-interactions, $\hat{\boldsymbol{q}}_{I_1} = \epsilon\hat{\boldsymbol{q}}'_{I_1} + \epsilon^2\hat{\boldsymbol{q}}''_{I_1}$, where $\hat{\boldsymbol{q}}''_{I_1} = f\hat{\boldsymbol{L}}^{-1}\hat{\boldsymbol{N}}_q^{I_1/I_1}$. Here $\hat{\boldsymbol{N}}_q^{I_1/I_1}$ stands for the nonlinear contribution due to the interaction of mode I_1 with itself (I_1 standing for either mode S or F), and it is computed as $\hat{\boldsymbol{N}}_q^{I_1/I_1} = \hat{\boldsymbol{N}}_q(\bar{\rho}, \bar{u}, \ldots; \hat{\rho}'_{I_1}\hat{u}'_{I_1}, \hat{\rho}'_{I_1}\hat{v}'_{I_1}, \ldots)$.

The streamwise distributions of the amplitude of the nonlinear interaction contribution (integrated in the wall-normal direction in the subsonic layer) are reported in figure 7 for the streamwise and wall-normal velocity modes and for the temperature mode, considering self-interactions (of the type S/S and F/F) and cross-interactions. For the latter, we consider both the initially unstable/initially stable mode interactions (S/F for $M = 4.5$ and F/S for $M = 5.5$) and the initially stable/initially unstable mode interactions (F/S for $M = 4.5$ and S/F for $M = 5.5$). In the figure, the nonlinear terms $\hat{N}_u$, $\hat{N}_v$ and $\hat{N}_T$ are normalized by the corresponding total time rate of change, namely $\int_0^{y_s} |\hat{N}_u|/|\hat{\mathrm{D}}\hat{u}/\mathrm{D}t|\,\mathrm{d}y$, $\int_0^{y_s} |\hat{N}_v|/|\hat{\mathrm{D}}\hat{v}/\mathrm{D}t|\,\mathrm{d}y$ and $\int_0^{y_s} |\hat{N}_T|/|\hat{\mathrm{D}}\hat{T}/\mathrm{D}t|\,\mathrm{d}y$.

The contributions to second-order modes resulting from the interactions of first-order modes are negligible for the $\hat{u}$ and $\hat{v}$ modes, and rather small for $\hat{T}$ modes. No significant changes occur as the modes evolve in the streamwise direction when crossing the synchronization location, and this for both self- and cross-interactions.

5. Governing equations for energy transfer analysis

Hypersonic boundary layer stability is characterized by the occurrence of fast and slow modes, whose spatial evolution depends on the thermal surface state and on the geometrical surface properties (Fedorov 2011; Fedorov & Tumin 2011). Temperature disturbances also play an important role in hypersonic boundary layer stability because of the energy exchanges between internal and kinetic disturbance energies (Zhu *et al.* 2018*b*). To elucidate the underlying physical mechanisms, and in particular to understand whether the mode spatial evolution is inviscid or viscous driven, we have analysed the transfer mechanisms between disturbance kinetic energy and temperature disturbance energy. In this process, the entropy (s), the disturbance kinetic energy (in the following, we use, respectively, the symbols k' and k'' to refer to the perturbation kinetic energy of the first- and second-order modes) and the temperature perturbation energy (similarly, we introduce k'_T and k''_T) play an important role. To unravel the role in the amplification/suppression of the effects of the wall thermal state, their evolutions are analysed in detail.

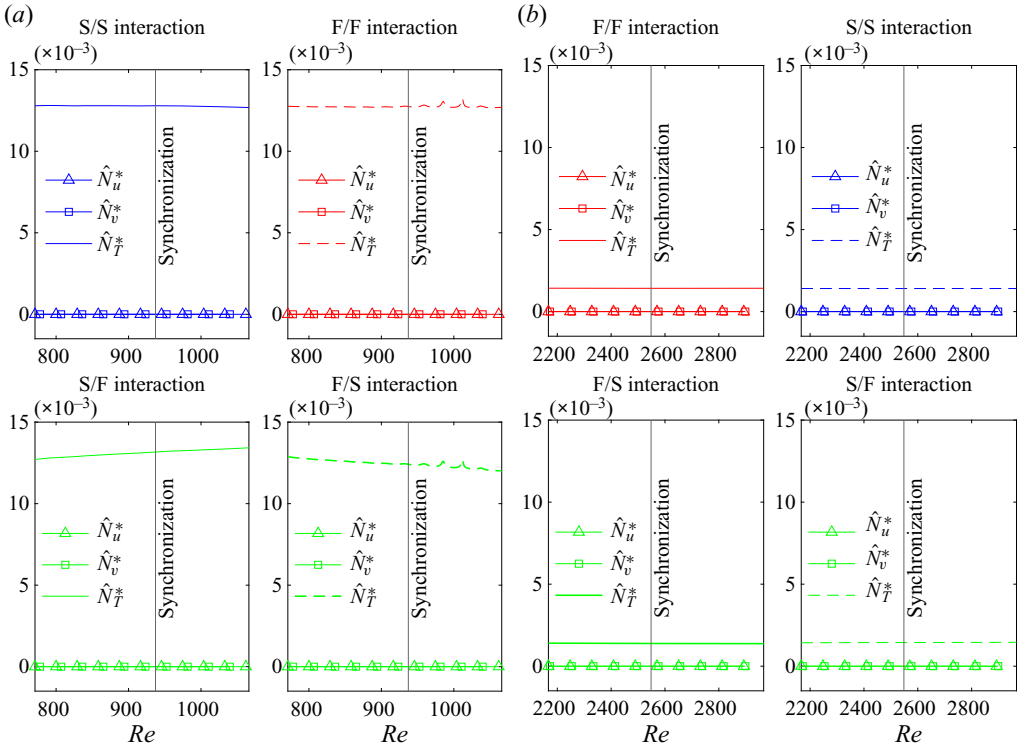

Figure 7. Streamwise distribution of the amplitude of the nonlinear interaction term integrated in the wall-normal direction at synchronization location: initially unstable ($M = 4.5$, S; $M = 5.5$; F)/initially stable mode ($M = 4.5$, F; $M = 5.5$; S) interaction ($M = 4.5$, S/F; $M = 5.5$; F/S) and initially stable ($M = 4.5$, F; $M = 5.5$; S)/initially unstable mode ($M = 4.5$, S; $M = 5.5$; F) interaction ($M = 4.5$, F/S; $M = 5.5$; S/F). Note that in the legend, $\hat{N}_u^*$, $\hat{N}_v^*$ and $\hat{N}_T^*$ stand for normalized quantities, namely $\int_0^{y_s} |\hat{N}_u|/|\hat{\mathrm{D}}\hat{u}/\mathrm{D}t|\,\mathrm{d}y$, $\int_0^{y_s} |\hat{N}_v|/|\hat{\mathrm{D}}\hat{v}/\mathrm{D}t|\,\mathrm{d}y$ and $\int_0^{y_s} |\hat{N}_T|/|\hat{\mathrm{D}}\hat{T}/\mathrm{D}t|\,\mathrm{d}y$. (*a*) $M = 4.5$; (*b*) $M = 5.5$.

5.1. *Entropy, kinetic energy and 'temperature energy' budgets*

In the following, we briefly derive the instantaneous governing equations for the entropy, the kinetic energy (k) and the 'temperature energy' variable (k_T). For the sake of the analysis, we introduce the dimensionless entropy variable $\tilde{s} = s/c_p$ defined as

$$\tilde{s} = \ln\left(\frac{T}{T_\infty}\right) - \frac{R}{c_p}\ln\left(\frac{p}{p_\infty}\right) + \tilde{s}_\infty. \tag{5.1}$$

The transport equation for $\tilde{s}$ is obtained by using the Gibbs relation that gives

$$\frac{\partial s}{\partial t} + u_j\frac{\partial s}{\partial x_j} = \underbrace{-\frac{1}{\rho c_p}\frac{\partial J_{s,j}}{\partial x_j}}_{\text{(i)}} + \underbrace{\frac{1}{c_p T}\phi}_{\text{(ii)}} + \underbrace{\frac{1}{c_p}\phi_T}_{\text{(iii)}}, \tag{5.2a}$$

with

$$J_{s,j} = -\frac{1}{T}\frac{\mu}{Pr}\frac{\partial T}{\partial x_j} \quad \text{and} \quad \rho\phi_T = J_{s,j}\left(-\frac{1}{T}\frac{\partial T}{\partial x_j}\right), \tag{5.2b}$$

where $\widetilde{()}$ has been dropped. Term (i) is the entropy diffusion flux associated with heat conduction, whereas terms (ii) and (iii) represent, respectively, the entropy production associated with viscous dissipation and energy exchanges by heat conduction.

The budget of the kinetic energy ($k = (u^2 + v^2 + w^2)/2$) is derived by taking the scalar product of the momentum budget and the velocity vector, yielding

$$\frac{\partial k}{\partial t} + u_j \frac{\partial k}{\partial x_j} = \underbrace{-\frac{\partial u_j p}{\partial x_j}}_{\text{(i)}} + \underbrace{\frac{p}{\rho}\frac{\partial u_j}{\partial x_j}}_{\text{(ii)}} + \underbrace{\frac{1}{\rho}\frac{\partial u_i \sigma_{ij}}{\partial x_j}}_{\text{(iii)}} \underbrace{-\phi}_{\text{(iv)}}. \tag{5.3}$$

The various terms on the right-hand side of (5.3) represent the pressure work (i), the pressure–dilatation (ii), the diffusion of kinetic energy (iii) and its dissipation due to viscous effects (iv). Introducing the energy variable (in a mathematical sense) $k_T = T^2/2$, its governing equation is derived by multiplying the internal energy budget (expressed in terms of T, (2.1c)) by the temperature, thus obtaining

$$\frac{\partial k_T}{\partial t} + u_j \frac{\partial k_T}{\partial x_j} = \underbrace{-\frac{1}{\rho c_v} T p \frac{\partial u_j}{\partial x_j}}_{\text{(i)}} + \underbrace{\frac{\gamma}{\rho Pr}\frac{\partial}{\partial x_j}\left(\mu \frac{\partial k_T}{\partial x_j}\right)}_{\text{(ii)}} + \underbrace{\frac{1}{c_v} T\phi}_{\text{(iii)}} \underbrace{-\phi_{k_T}}_{\text{(iv)}}, \tag{5.4a}$$

with

$$\phi_{k_T} = \frac{\gamma}{Pr}\nu\left(\frac{\partial T}{\partial x_j}\right)^2. \tag{5.4b}$$

The terms on the right-hand side of (5.4a) represent the contribution due to pressure–dilatation (i), the exchange due to heat conduction (ii), the production associated with viscous dissipation of kinetic energy (iii) and the effects of thermal power dissipation associated with heat conduction (iv).

Inspection of (5.2a), (5.3) and (5.4a) shows the following:

(i) Pressure–dilatation (terms (ii) of (5.3) and (i) of (5.4a)) is a reversible inviscid energy transfer mechanism and it has an increasingly important role as the Mach number increases.

(ii) The action of viscous forces is an irreversible energy transfer mechanism (i.e. associated with entropy production through term (iii) of (5.2a)) that has a tendency to suppress mechanical energy (through term (iv) of (5.3)) and to amplify the energy variable k_T (term (iii) of (5.4a)), and its effect increases with the Mach number (having an impact on the scales, and hence on the receptivity of the boundary layer).

(iii) The energy exchange due to heat conduction is an irreversible process (term (ii) of (5.2a)) whose action is toward suppressing k_T (term (iv) of (5.4a)).

5.2. *Governing equations for the entropy disturbances, the disturbance kinetic energy and temperature disturbance energy*

To shed some light on the physical mechanisms driving early-stage disturbance evolution and the associated energy transfer mechanisms, we have analysed the budgets of the entropy disturbances and of the disturbance kinetic and temperature disturbance energies up to second order.

5.2.1. *Entropy disturbances*

To derive the equations for the entropy disturbances, we first expand the thermodynamic (5.1) and the constitutive (5.2) relations up to second order, thus obtaining

$$\bar{s} = \ln\left(\frac{\bar{T}}{T_\infty}\right) - \frac{R}{c_p}\ln\left(\frac{\bar{p}}{p_\infty}\right) + \bar{s}_\infty, \quad \bar{J}_{s,j} = -\frac{1}{\bar{T}}\frac{\bar{\mu}}{Pr}\frac{\partial \bar{T}}{\partial x_j}, \tag{5.5a}$$

$$s' = \frac{T'}{\bar{T}} - \frac{R}{c_p}\frac{p'}{\bar{p}}, \quad J_{s',j} = -\frac{\bar{\mu}}{Pr}\frac{\partial}{\partial x_j}\left(\frac{T'}{\bar{T}}\right) = J'_{s,j}, \tag{5.5b}$$

$$s'' = \frac{T''}{\bar{T}} - \frac{R}{c_p}\frac{p''}{\bar{p}} - \frac{1}{2}\left[\left(\frac{T'}{\bar{T}}\right)^2 - \frac{R}{c_p}\left(\frac{p'}{\bar{p}}\right)^2\right], \quad J_{s'',j} = J''_{s,j} + \frac{\bar{\mu}}{2Pr}\frac{\partial}{\partial x_j}\left(\frac{T'}{\bar{T}}\right)^2. \tag{5.5c}$$

The governing equations for the entropy disturbances are then obtained introducing the second-order decomposition in (5.2*a*) and using (5.5*a*)–(5.5*c*), thus giving

$$\begin{aligned}\frac{\partial s^{(n)}}{\partial t} + \bar{u}_j\frac{\partial s^{(n)}}{\partial x_j} = {} & \frac{\bar{\nu}}{Pr}\frac{\partial^2}{\partial x_j^2}\left(\frac{T^{(n)}}{\bar{T}}\right) + \frac{1}{Pr\bar{\rho}}\frac{\partial}{\partial x_j}\left(\frac{T^{(n)}}{\bar{T}}\right)\frac{\partial \bar{\mu}}{\partial x_j} \\ & + \frac{1}{c_p\bar{T}}\phi_L^{(n)} + \frac{1}{Pr\bar{T}}\phi_{T,L}^{(n)} - \frac{1}{\bar{\rho}}(\rho^{(n)}\bar{u}_j + \bar{\rho}u_j^{(n)})\frac{\partial \bar{s}}{\partial x_j} \\ & + (n-1)f(N_{B,s}^{(n)} + N_{S,s}^{(n)}),\end{aligned} \tag{5.6}$$

where $n = 1, 2$, and

$$\phi_{T,L}^{(n)} = 2\bar{\nu}\left(\frac{1}{\bar{T}}\frac{\partial \bar{T}}{\partial x_j}\right)\frac{\partial}{\partial x_j}\left(\frac{T^{(n)}}{\bar{T}}\right) \tag{5.7}$$

is the linearized thermal power dissipation (associated with heat conduction). The terms $N_{B,s}^{(n)}$ and $N_{S,s}^{(n)}$ account for the nonlinear contributions associated with lower-order-mode interactions. For $n = 1$, $N_{B,s}^{(1)} = 0$ and $N_{S,s}^{(1)} = 0$; for $n = 2$,

$$N_{B,s}^{(2)} = -\frac{\rho'}{\bar{\rho}}\frac{\partial s'}{\partial t} - \frac{1}{\bar{\rho}}(\rho'\bar{u}_j + \bar{\rho}u'_j)\frac{\partial s'}{\partial x_j} - \frac{\rho'}{\bar{\rho}}u'_j\frac{\partial \bar{s}}{\partial x_j}, \tag{5.8a}$$

$$N_{S,s}^{(2)} = \frac{1}{c_p\bar{T}}\left[\phi' - \frac{T'}{\bar{T}}\phi'_L + \frac{1}{2}\left(\frac{T'}{\bar{T}}\right)^2\bar{\phi}\right] - \frac{1}{2Pr}\frac{\partial}{\partial x_j}\left[\bar{\mu}\frac{\partial}{\partial x_j}\left(\frac{T'}{\bar{T}}\right)^2\right], \tag{5.8b}$$

with $\bar{\phi} = \bar{\nu}[2\bar{S}_{ij}\bar{S}_{ij} - \frac{2}{3}\bar{S}_{\ell\ell}\bar{S}_{kk}]$ the base flow dissipation.

Dropping superscript (n) (unless confusion arises) and introducing the normal-mode expansion in (5.6), gives

$$\frac{\hat{\mathrm{D}}\hat{s}}{\mathrm{D}t} + \bar{v}\frac{\mathrm{d}\hat{s}}{\mathrm{d}y} = D_s + \hat{\phi}_{s,u} + \hat{\phi}_{s,T} + s\text{-}mgP + (n-1)f\hat{N}_s, \tag{5.9}$$

where D_s and s-mgP represent, respectively, the normal-mode forms of the diffusion and the base flow entropy gradient generation contributions, and $\hat{\phi}_{s,u}$ and $\hat{\phi}_{s,T}$ are the normal-mode form of the entropy generation rates associated with viscous and heat

conduction effects, with

$$D_s = \frac{\bar{\nu}}{Pr}\left[\left(\alpha^2 - \mathrm{i}\frac{\mathrm{d}\alpha}{\mathrm{d}x}\right)\frac{\hat{T}}{\bar{T}} + 2\mathrm{i}\alpha\hat{T}\frac{\partial}{\partial x}\left(\frac{1}{\bar{T}}\right) + \hat{T}\frac{\partial^2}{\partial x^2}\left(\frac{1}{\bar{T}}\right) + \frac{1}{\bar{T}}\frac{\mathrm{d}^2\hat{T}}{\mathrm{d}y^2} + 2\frac{\mathrm{d}\hat{T}}{\mathrm{d}y}\frac{\partial}{\partial y}\left(\frac{1}{\bar{T}}\right) + \hat{T}\frac{\partial^2}{\partial y^2}\left(\frac{1}{\bar{T}}\right)\right] + \frac{1}{Pr}\frac{1}{\bar{\rho}}\left[\mathrm{i}\alpha\frac{\hat{T}}{\bar{T}} + \hat{T}\frac{\partial}{\partial x}\left(\frac{1}{\bar{T}}\right)\right]\frac{1}{\bar{T}}\frac{\partial\bar{\mu}}{\partial x} + \frac{1}{Pr}\frac{1}{\bar{\rho}}\left[\frac{1}{\bar{T}}\frac{\mathrm{d}\hat{T}}{\mathrm{d}y} + \hat{T}\frac{\partial}{\partial y}\left(\frac{1}{\bar{T}}\right)\right]\frac{\partial\bar{\mu}}{\partial y}, \tag{5.10a}$$

$$s\text{-}mgP = -\left[\hat{u} + \bar{u}\left(\frac{\hat{p}}{\bar{p}} - \frac{\hat{T}}{\bar{T}}\right)\right]\frac{\partial\bar{s}}{\partial x} - \left[\hat{v} + \bar{v}\left(\frac{\hat{p}}{\bar{p}} - \frac{\hat{T}}{\bar{T}}\right)\right]\frac{\partial\bar{s}}{\partial y}, \tag{5.10b}$$

$$\hat{\phi}_{s,u} = \frac{1}{c_p\bar{T}}\hat{\phi}_L, \tag{5.10c}$$

$$\hat{\phi}_{s,T} = \frac{1}{\bar{T}}\hat{\phi}_{T,L}, \tag{5.10d}$$

where

$$\hat{\phi}_{T,L} = 2\frac{\bar{\nu}}{Pr}\left\{\left[\frac{1}{\bar{T}}\frac{\partial\bar{T}}{\partial x}\frac{1}{\bar{T}}i\alpha\hat{T} + \hat{T}\frac{\partial}{\partial x}\left(\frac{1}{\bar{T}}\right)\right] + \left[\frac{1}{\bar{T}}\frac{\partial\bar{T}}{\partial y}\frac{1}{\bar{T}}\frac{\mathrm{d}\hat{T}}{\mathrm{d}y} + \hat{T}\frac{\partial}{\partial y}\left(\frac{1}{\bar{T}}\right)\right]\right\} \tag{5.11}$$

and $\hat{\phi}_L$ is defined in (4.16*d*). Terms $\hat{N}_{B,s}$ and $\hat{N}_{S,s}$ are the normal-mode forms of the mode interaction terms:

$$\hat{N}_{B,s} = \mathrm{i}\omega\frac{\hat{\rho}'}{\bar{\rho}}\hat{s}' - \mathrm{i}\alpha\frac{1}{\bar{\rho}}(\hat{\rho}'\bar{u} + \bar{\rho}\hat{u}')\hat{s}' - \frac{1}{\bar{\rho}}(\hat{\rho}'\bar{v} + \bar{\rho}\hat{v}')\frac{\mathrm{d}\hat{s}'}{\mathrm{d}y} - \frac{\hat{\rho}'}{\bar{\rho}}\hat{u}'\frac{\partial\bar{s}}{\partial x} - \frac{\hat{\rho}'}{\bar{\rho}}\hat{v}'\frac{\partial\bar{s}}{\partial y}, \tag{5.12a}$$

$$\hat{N}_{S,s} = \frac{1}{c_p\bar{T}}\left[\hat{\phi}' - \frac{\hat{T}'}{\bar{T}}\hat{\phi}'_L + \frac{1}{2}\left(\frac{\hat{T}'}{\bar{T}}\right)^2\bar{\phi}\right] - \frac{1}{2Pr}\frac{\partial}{\partial x_j}\left[\bar{\mu}\frac{\partial}{\partial x_j}\left(\frac{\hat{T}'}{\bar{T}}\right)^2\right]. \tag{5.12b}$$

Note that unless otherwise specified, here and in the following $\widehat{(\cdot)}$ stands for either the first- or the second-order mode, respectively.

5.2.2. *Disturbance kinetic energy*

Let $\hat{k}'$ and $\hat{k}''$ be the disturbance kinetic energy, respectively, of the first- and second-order velocity disturbance mode. Defining $\hat{k}' = \mathscr{R}(\hat{u}'_i)\mathscr{R}(\hat{u}'_i)/2$ and $\hat{k}'' = \mathscr{R}(\hat{u}''_i)\mathscr{R}(\hat{u}''_i)/2$, $\mathscr{R}(\cdot)$ denoting the real part, the governing equations for the disturbance kinetic energies are readily obtained by multiplying the real part of the nth-order normal-mode form of (3.13*b*) by the real part of the nth-order velocity disturbance mode $\mathscr{R}(\hat{u}_i^{(n)})$. Dropping superscript

(n), one has

$$\mathscr{R}(\hat{u}_i)\mathscr{R}\left[\frac{\partial \hat{u}_i}{\partial t}+\bar{u}_j\frac{\partial \hat{u}_i}{\partial x_j}+\frac{1}{\bar{\rho}}\frac{\partial \hat{p}}{\partial x_i}-\frac{1}{\bar{\rho}}\frac{\partial \hat{\sigma}_{ij}}{\partial x_j}+\frac{1}{\bar{\rho}}(\hat{\rho}\bar{u}_j+\bar{\rho}\hat{u}_j)\frac{\partial \bar{u}_i}{\partial x_j}\right]=(n-1)\mathscr{R}(\hat{u}_i)\mathscr{R}(f\hat{N}_{u_i}). \tag{5.13}$$

The governing equation for $\hat{k}$ ($\hat{k}$ standing for either $\hat{k}'$ or $\hat{k}''$) is then written as

$$\frac{\hat{\mathrm{D}}\hat{k}}{\mathrm{D}t}+\bar{v}\frac{\mathrm{d}\hat{k}}{\mathrm{d}y}=-\frac{1}{\bar{\rho}}\Pi_W+\frac{1}{\bar{\rho}}\Pi_\theta+D_k-\phi+P_k+(n-1)\hat{\mathscr{N}}_k, \tag{5.14}$$

where Π_W, Π_θ, D_k, ϕ and P_k are, respectively, the disturbance pressure work, the pressure–dilatation, the diffusion of disturbance kinetic energy and its dissipation due to viscous effects and the production resulting from base flow/mode interaction driven by mean velocity gradients:

$$\Pi_W=\frac{\partial}{\partial x_i}[\mathscr{R}(\hat{p})\mathscr{R}(\hat{u}_i)], \tag{5.15a}$$

$$\Pi_\theta=\mathscr{R}(\hat{p})\frac{\partial}{\partial x_i}[\mathscr{R}(\hat{u}_i)], \tag{5.15b}$$

$$D_k=\frac{1}{\bar{\rho}}\frac{\partial}{\partial x_i}[\mathscr{R}(\hat{u}_i)\mathscr{R}(\hat{\sigma}_{ij})], \tag{5.15c}$$

$$\phi=\frac{1}{\bar{\rho}}\mathscr{R}(\hat{S}_{ij})\mathscr{R}(\hat{\sigma}_{ij}), \tag{5.15d}$$

$$P_k=-\frac{1}{\bar{\rho}}\{\mathscr{R}(\hat{u}_i)[\mathscr{R}(\hat{\rho})\bar{u}_j+\bar{\rho}\mathscr{R}(\hat{u}_j)]\}\frac{\partial \bar{u}_i}{\partial x_j}. \tag{5.15e}$$

The term $\hat{\mathscr{N}}_k$ is the contribution to the higher-order disturbance kinetic energy resulting from first-order mode interactions, defined as

$$\hat{\mathscr{N}}_k=\mathscr{R}(\hat{u}_i)\mathscr{R}(f\hat{N}_{u_i}), \tag{5.16}$$

with

$$\hat{N}_{u_i}=\frac{1}{\bar{\rho}}\left[\mathrm{i}\omega\hat{\rho}'\hat{u}_i'-\mathrm{i}\alpha(\hat{\rho}'\bar{u}+\bar{\rho}\hat{u}')\hat{u}_i'-(\hat{\rho}'\bar{v}+\bar{\rho}\hat{v}')\frac{\mathrm{d}\hat{u}_i'}{\mathrm{d}y}-\hat{\rho}'\hat{u}'\frac{\partial \overline{u_i}}{\partial x}-\hat{\rho}'\hat{v}'\frac{\partial \overline{u_i}}{\partial y}\right]. \tag{5.17}$$

5.2.3. *Temperature disturbance energy*

Let $\hat{k}_T'$ and $\hat{k}_T''$ be the temperature disturbance energy, respectively, of the first- and second-order temperature disturbance mode. Defining $\hat{k}_T'=\mathscr{R}(\hat{T}')\mathscr{R}(\hat{T}')/2$ and $\hat{k}_T''=\mathscr{R}(\hat{T}'')\mathscr{R}(\hat{T}'')/2$, the governing equations for the temperature disturbance energies are readily obtained by multiplying the real part of the nth-order normal-mode form of (3.13*c*) by the real part of the nth-order temperature disturbance mode $\mathscr{R}(\hat{T}^{(n)})$. Dropping

superscript (n), one has

$$\mathscr{R}(\hat{T})\mathscr{R}\left\{\frac{\partial \hat{T}}{\partial t}+\bar{u}_j\frac{\partial \hat{T}}{\partial x_j}+\frac{1}{\bar{\rho}c_v}\left[\hat{p}\frac{\partial \bar{u}_i}{\partial x_i}+\bar{p}\frac{\partial \hat{u}_i}{\partial x_i}\right]-\frac{\gamma}{Pr\bar{\rho}}\frac{\partial}{\partial x_j}\left[\bar{\mu}\frac{\partial \hat{T}}{\partial x_j}\right]\right\}$$
$$+\mathscr{R}(\hat{T})\mathscr{R}\left\{-\frac{1}{c_v}\hat{\phi}_L+\frac{1}{\bar{\rho}}\left[\hat{\rho}\bar{u}_j+\bar{\rho}\hat{u}_j\right]\frac{\partial \bar{T}}{\partial x_j}\right\}=(n-1)\mathscr{R}(\hat{T})\mathscr{R}(f\hat{N}_T). \tag{5.18}$$

The governing equation for $\hat{k}_T$ ($\hat{k}_T$ standing for either $\hat{k}'_T$ or $\hat{k}''_T$) is then written as

$$\frac{\hat{\mathrm{D}}\hat{k}_T}{\mathrm{D}t}+\bar{v}\frac{\mathrm{d}\hat{k}_T}{\mathrm{d}y}=-\frac{1}{\bar{\rho}}\Pi_{\theta,T}+D_{k_T}+\phi_u-\phi_{k_T}+P_{k_T}+(n-1)\hat{\mathscr{N}}_{k_T}, \tag{5.19}$$

where $\Pi_{\theta,T}$, D_{k_T}, ϕ_u, ϕ_{k_T} and P_{k_T} are, respectively, the (normal-mode form of the) temperature disturbance energy transfer associated with pressure–dilatation, the exchange of temperature disturbance energy due to heat conduction, the production due to viscous effects, the thermal power temperature disturbance energy loss and the production resulting from base flow/mode interaction driven by mean temperature gradients:

$$\Pi_{\theta,T}=\frac{1}{c_v}\mathscr{R}(\hat{T})\mathscr{R}\left(\hat{p}\frac{\partial \bar{u}_i}{\partial x_i}+\bar{p}\frac{\partial \hat{u}_i}{\partial x_i}\right), \tag{5.20a}$$

$$D_{k_T}=\frac{\gamma}{Pr}\frac{1}{\bar{\rho}}\frac{\partial}{\partial x_j}\left[\mathscr{R}(\hat{T})\bar{\mu}\mathscr{R}\left(\frac{\partial \hat{T}}{\partial x_j}\right)\right], \tag{5.20b}$$

$$\phi_u=\frac{1}{c_v}\mathscr{R}(\hat{T})\mathscr{R}(\hat{\phi}_L), \tag{5.20c}$$

$$\phi_{k_T}=\frac{\gamma}{Pr}\bar{\nu}\frac{\partial \mathscr{R}(\hat{T})}{\partial x_j}\frac{\partial \mathscr{R}(\hat{T})}{\partial x_j}, \tag{5.20d}$$

$$P_{k_T}=-\frac{1}{c_v\bar{\rho}}\mathscr{R}(\hat{T})[\mathscr{R}(\hat{\rho}\bar{u}_j+\bar{\rho}\hat{u}_j)]\frac{\partial \bar{T}_i}{\partial x_j}. \tag{5.20e}$$

The term $\hat{\mathscr{N}}_{k_T}$ is the contribution to the higher-order temperature disturbance energy resulting from first-order mode interactions, defined as

$$\hat{\mathscr{N}}_{k_T}=\mathscr{R}(\hat{T})\mathscr{R}(f\hat{N}_T), \tag{5.21}$$

with

$$\hat{N}_T=\frac{1}{\bar{\rho}c_v}\left[\mathrm{i}\omega\hat{\rho}'\hat{T}'-\mathrm{i}\alpha(\hat{\rho}'\bar{u}+\bar{\rho}\hat{u}')\hat{T}'-(\hat{\rho}'\bar{v}+\bar{\rho}\hat{v}')\frac{\mathrm{d}\hat{T}'}{\mathrm{d}y}-\hat{\rho}'\hat{u}'\frac{\partial \bar{T}}{\partial x}-\hat{\rho}'\hat{v}'\frac{\partial \bar{T}}{\partial y}\right]$$
$$-\frac{1}{\bar{\rho}c_v}\hat{p}'\left(\mathrm{i}\alpha\hat{u}'+\frac{\mathrm{d}\hat{v}'}{\mathrm{d}y}\right)+\frac{1}{c_v}\hat{\phi}'. \tag{5.22a}$$

Unless confusion arises, in the following $\mathscr{R}(\cdot)$ is omitted for ease of reading. Equations (5.14) and (5.19) show that at higher order, the disturbance kinetic and temperature disturbance energies are driven not only by inviscid mechanisms associated with dilatational effects, base flow/disturbance interaction and the combined actions of viscous and heat conduction effects (as for the lower-order case), but also by velocity, pressure

and temperature mode interactions. The equations show that disturbance kinetic energy is drained by the action of viscous dissipation ϕ, whereas temperature disturbance energy is produced by the action of linearized viscous dissipation (term $\hat{T}\hat{\phi}_L/c_v$ of (5.20*c*)) and is dissipated by heat conduction effects (term ϕ_{k_T}).

5.2.4. *Near-wall disturbance entropy and perturbation energy behaviour*

In the near-wall vicinity, the entropy, the perturbation kinetic energy and the temperature perturbation energy equations (5.6), (5.14) and (5.19) reduce to

$$-\mathrm{i}\omega\hat{s} = \frac{1}{Pr}\frac{1}{\bar{\rho}}\frac{\partial}{\partial y}\left[\bar{\mu}\frac{\mathrm{d}}{\mathrm{d}y}\left(\frac{\hat{T}}{\bar{T}}\right)\right] + \frac{1}{c_p\bar{T}}\hat{\phi}_L + \frac{1}{\bar{T}}\hat{\phi}_{T,L}, \tag{5.23a}$$

$$\frac{\partial}{\partial y}\left(\bar{\mu}\frac{\mathrm{d}\hat{k}}{\mathrm{d}y}\right) = \bar{\rho}\phi, \tag{5.23b}$$

$$\frac{\gamma}{Pr}\frac{\partial}{\partial y}\left(\bar{\mu}\frac{\mathrm{d}\hat{k}_T}{\mathrm{d}y}\right) = \bar{\rho}\phi_{k_T}, \tag{5.23c}$$

where

$$\left.\begin{aligned}
\hat{\phi}_L &= 2\bar{\nu}\left[\frac{4}{3}\frac{\partial\bar{v}}{\partial y}\mathscr{R}\left(\frac{\mathrm{d}\hat{v}}{\partial y}\right) + \frac{\partial\bar{u}}{\partial y}\mathscr{R}\left(\frac{\mathrm{d}\hat{u}}{\partial y}\right)\right],\\
\hat{\phi}_{T,L} &= 2\frac{\bar{\nu}}{Pr}\left[\frac{1}{\bar{T}}\frac{\partial\bar{T}}{\partial y}\frac{1}{\bar{T}}\mathscr{R}\left(\frac{\mathrm{d}\hat{T}}{\partial y}\right)\right],\\
\phi &= \bar{\nu}\left[\mathscr{R}\left(\frac{\mathrm{d}\hat{u}}{\partial y}\right)\mathscr{R}\left(\frac{\mathrm{d}\hat{u}}{\partial y}\right) + \frac{4}{3}\mathscr{R}\left(\frac{\mathrm{d}\hat{v}}{\partial y}\right)\mathscr{R}\left(\frac{\mathrm{d}\hat{v}}{\partial y}\right)\right],\\
\phi_{k_T} &= \frac{\gamma}{Pr}\bar{\nu}\mathscr{R}\left(\frac{\mathrm{d}\hat{T}}{\partial y}\right)\mathscr{R}\left(\frac{\mathrm{d}\hat{T}}{\partial y}\right).
\end{aligned}\right\} \tag{5.24}$$

Equations (5.23*a*)–(5.23*c*) show that at the wall

(i) there is no direct effect of mode interactions on both k and k_T;
(ii) dissipation and diffusive transport of perturbation kinetic energy are in equilibrium; and
(iii) thermal power dissipation and transport associated with heat conduction of temperature perturbation energy are in equilibrium.

6. Energy analysis

6.1. *Perturbation energy analysis*

The discussion being centred on the understanding of the underlying energy transfer mechanisms, we scrutinize the contributions associated with the pressure–dilatation and the dissipation due to viscous and heat conduction effects on the perturbation kinetic energy and the temperature perturbation energy. In addition, to ascertain the role of the

reversible versus the irreversible mechanisms we have also analysed in detail these effects on the entropy perturbation. For clarity, the terms that have been scrutinized are

$$\text{in the budget of } s: \quad \phi_{s,u} = \frac{1}{c_p \bar{T}} \hat{T} \phi_L, \quad \phi_{s,T} = \frac{1}{Pr \bar{T}} \hat{\phi}_{T,L}; \tag{6.1a}$$

$$\text{in the budget of } \hat{k}: \quad \hat{p}\hat{\theta}, \quad -\phi_{S^2}, \quad -\phi_{\theta^2}; \tag{6.1b}$$

$$\text{in the budget of } \hat{k}_T: \quad -\frac{1}{c_v} \hat{T}(p\theta)_L, \quad \phi_u = \frac{1}{c_v} \hat{T} \phi_L, \quad -\phi_{k_T}, \tag{6.1c}$$

$$\text{with} \quad \bar{\rho}\phi_{S^2} = 2\bar{\mu}\mathscr{R}(\hat{S}_{ij})\mathscr{R}(\hat{S}_{ij}), \quad \bar{\rho}\phi_{\theta^2} = -\frac{2}{3}\bar{\mu}\mathscr{R}(\hat{\theta})\mathscr{R}(\hat{\theta}). \tag{6.1d}$$

Observe that the linearized thermal power dissipation $\hat{\phi}_{T,L}$ (equation (5.11)) can in principle attain either non-negative or non-positive values, and, consequently, entropy perturbation can either increase or decrease due to (linearized) heat conduction. Similarly, entropy perturbation can either increase or decrease by the action of the linearized viscous dissipation, since $\hat{\phi}_L$ (equation (4.16*d*)) can in principle be either non-negative or non-positive. As also proposed in Zhu *et al.* (2020, 2021), the dissipation of mechanical energy is expressed as the sum of two terms ($\phi = \phi_{S^2} + \phi_{\theta^2}$), where ϕ_{S^2} accounts for the deformation work associated with the deformation tensor and ϕ_{θ^2} represents the contribution due to dilatational effects (equation (6.1*d*)). Observe that $\phi_{S^2} \geq 0$ (i.e. k is dissipated due to the action of deformation work), whereas $\phi_{\theta^2} \leq 0$ (i.e. k is produced due to dilatational viscous dissipation effects).

The budgets of the slow and fast entropy perturbation modes are reported in figure 8. The figure shows that the primary physical mechanisms driving the entropy perturbation evolution are its diffusion (associated with heat conduction) and the base flow entropy gradient generation (*s-mgP*). The (linearized) viscous ($(1/c_p\bar{T})\hat{\phi}_L$) and thermal power ($(1/\bar{T})\hat{\phi}_{T,L}$) dissipation contributions (in the discussion that follows their sum is also referred to as the entropy generation rate) are negligible except in very close proximity to the wall (but still small), where diffusion dominates. Across the critical layer, entropy perturbation is primarily controlled by mean base flow entropy gradient production, by transverse convection and diffusion and, to a lesser extent, by viscous dissipation (the latter contribution being somewhat more significant for the fast mode). Across the critical layer, diffusion plays a significant role in the slow (fast) mode for adiabatic (cold) wall.

The streamwise distributions of the generation rates integrated separately over the subsonic sublayer (in the range $[0, y_s]$; this region is hereafter simply referred to as the subsonic region, *Sub*) and over the supersonic portion of the boundary layer above the sonic line (in the range $[y_s, \delta]$, δ being the local boundary layer height; this region is hereafter simply referred to as the supersonic region, *Sup*) are reported in figure 9. The contribution of term *s-mgP* (results not reported in the figure for clarity) is dominant, further confirming that dissipative effects are rather negligible. In the supersonic region (for both modes S and F), the generation rates are not in phase, whereas they are in phase in the subsonic portion of the boundary layer. In the subsonic region, for adiabatic wall, the contribution resulting from the effects due to viscous dissipation is more significant than that due to thermal power dissipation. The opposite holds true for cold wall.

In conclusion, entropy perturbations are driven primarily by an inviscid mechanism associated with base flow entropy gradient production (as already pointed out in the discussion of the entropy perturbation budgets at synchronization location). This indicates that to a good approximation, in the subsonic layer, where acoustic waves are trapped

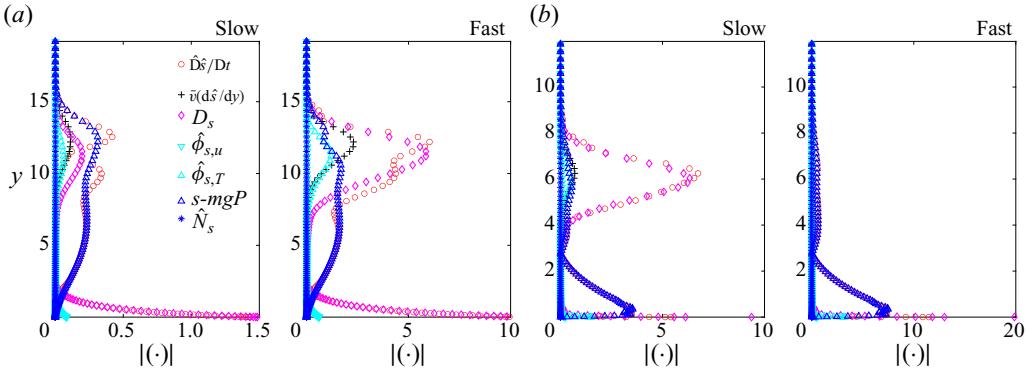

Figure 8. Budgets of the entropy perturbation of modes S and F for (*a*) adiabatic wall ($M = 4.5$) and (*b*) cold wall ($M = 5.5$).

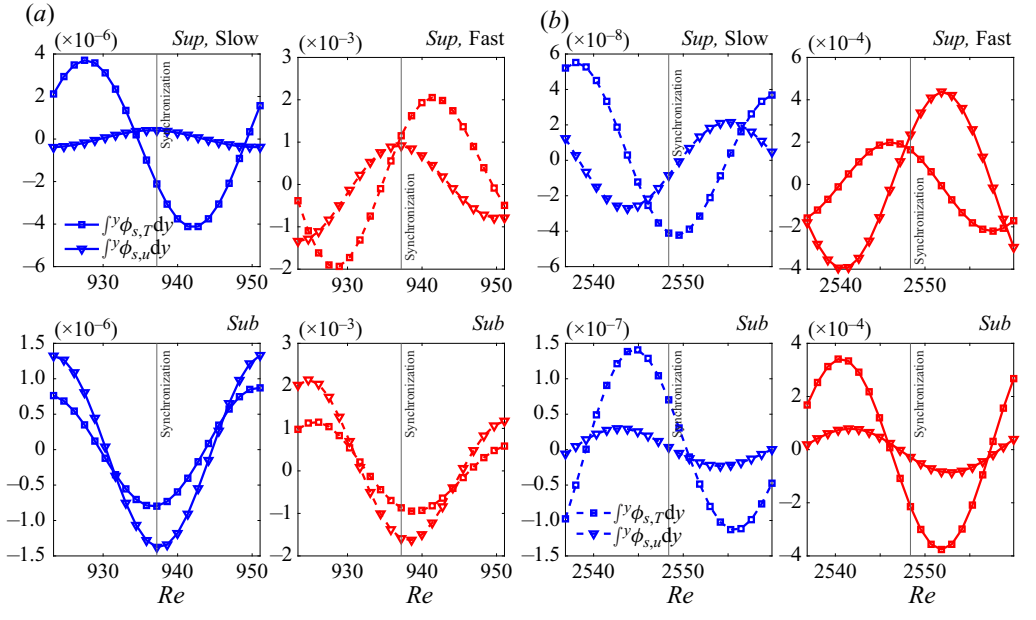

Figure 9. Streamwise distributions of the entropy generation rate of modes S and F integrated in the wall-normal direction across the supersonic (*Sup*) and subsonic (*Sub*) regions. The rates are normalized by $\max_x[\int^y |\partial s/\partial t + \bar{u}\partial s/\partial x|\, dy]$. (*a*) $M = 4.5$; (*b*) $M = 5.5$.

(Mack 1984; Fedorov 2011; Zhong & Wang 2012), the exchange of energy is a reversible process associated with pressure–dilatation.

The wall-normal budgets of the perturbation kinetic energy and of the temperature perturbation energy in the subsonic portion of the boundary layer at synchronization location are reported, respectively, in figures 10 and 11. Figure 10 shows that the perturbation kinetic energy is driven by the pressure work, pressure–dilation and base flow/perturbation interaction mechanisms. The slow mode undergoes positive pressure work near the wall, which changes sign moving away from the wall becoming negative at about 1/3 of the subsonic thickness. The pressure–dilatation term is predominantly negative draining perturbation kinetic energy. For mode F, the pressure work is negative

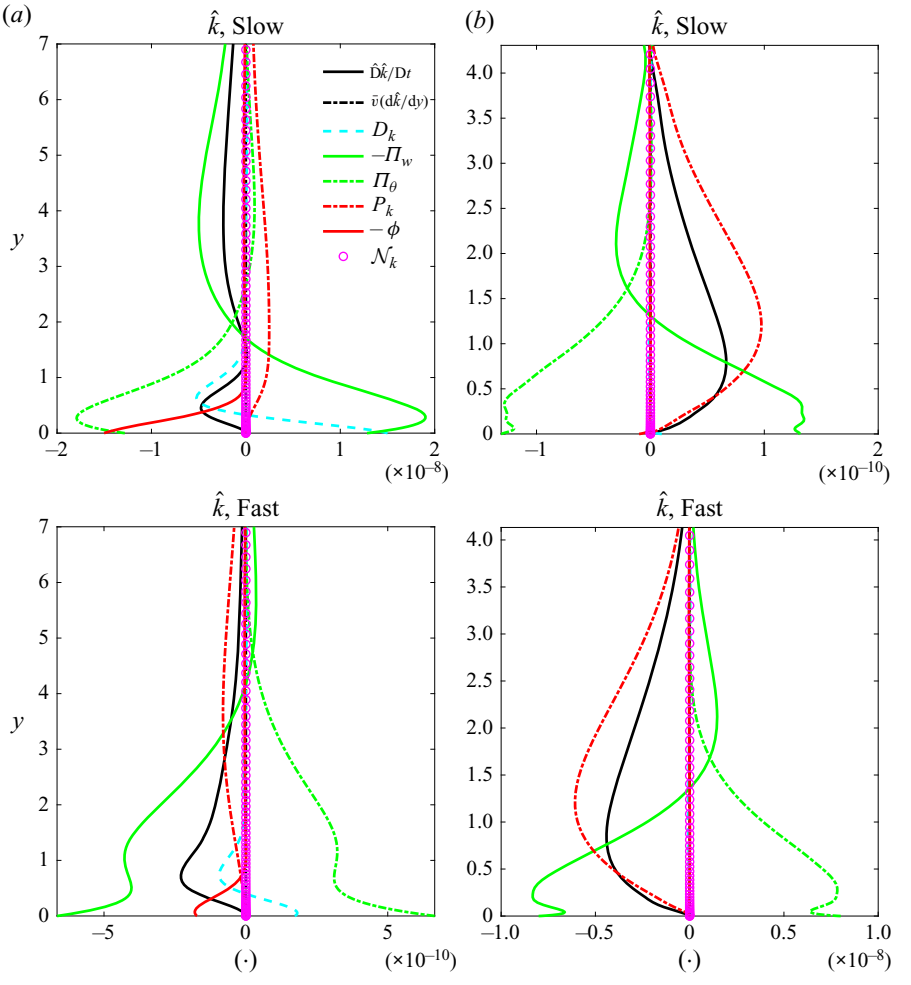

Figure 10. Perturbation kinetic energy budget of modes S and F at synchronization location. (*a*) $M = 4.5$; (*b*) $M = 5.5$.

near the wall and the pressure–dilatation is positive contributing to an increase of its perturbation kinetic energy. As in fully turbulent boundary layers, and in agreement with (5.23*b*), dissipation and diffusion of perturbation kinetic energy by viscous effects are in equilibrium at the wall. The budget of the temperature perturbation energy (figure 11) shows that thermal power dissipation and the exchanges associated with heat conduction are significant in the proximity of the wall, the two being in equilibrium at the wall (as predicted from (5.23*c*)).

To better understand the underlying inviscid energy transfer mechanisms, we have scrutinized in more detail the dilatation and dissipation rates associated with viscous and heat conduction effects. Figure 12 reports the streamwise distributions of $\hat{p}\hat{\theta}$ and $-\hat{T}(p\theta)_L/c_v$ for the adiabatic and cold-wall cases ($M = 4.5$ and $M = 5.5$, respectively) at $y = 1/8y_s$ and y_{crit}. As also found by Zhu *et al.* (2020, 2021), the pressure–dilatation exhibits a nearly sinusoidal variation in the streamwise direction alternating between positive and negative values, and changes sign also in the wall-normal direction. For $M =$

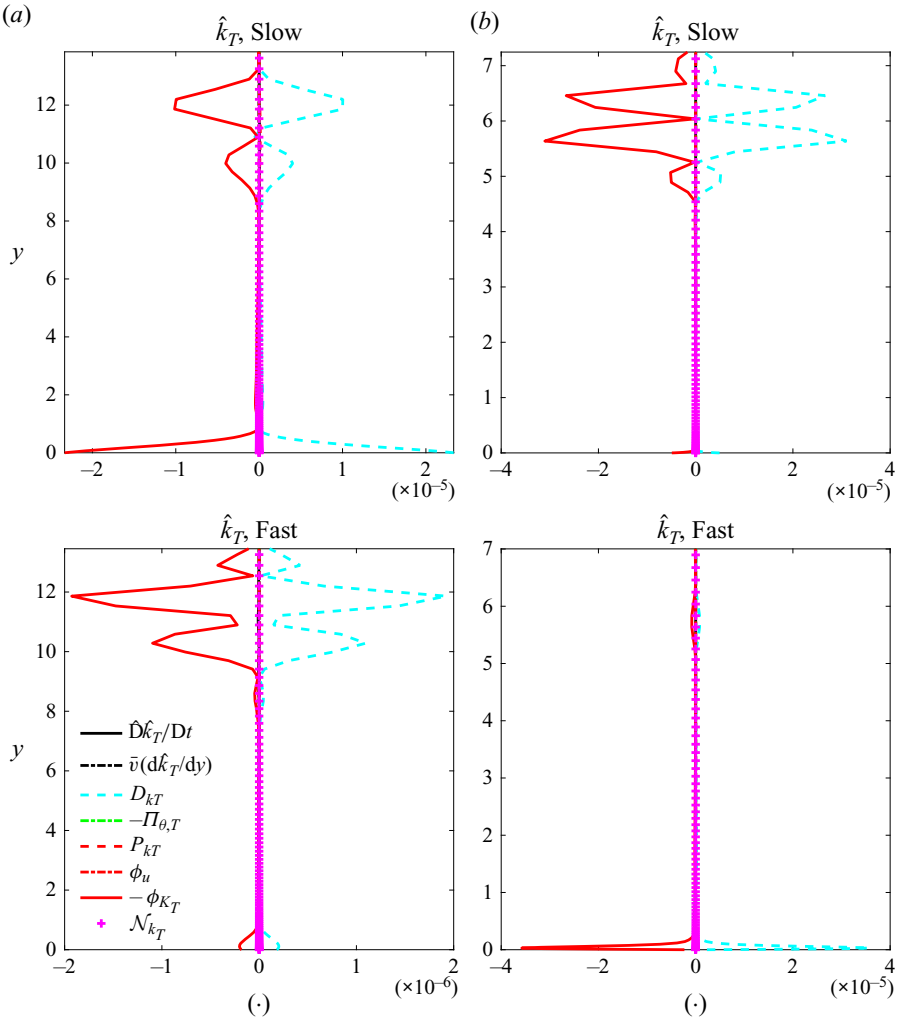

Figure 11. Temperature perturbation energy budget of modes S and F at synchronization location. (*a*) $M = 4.5$; (*b*) $M = 5.5$.

4.5 (and $M = 6$ and $M = 6.5$ cases, not reported) the slow mode (which is the initially unstable mode for these cases) experiences energy exchanges that grow in amplitude in the streamwise direction, whereas the fast mode undergoes a decaying energy exchange mechanism. The opposite holds true for $M = 5.5$, for which the fast mode is initially unstable. The same features are observed for $-\hat{T}(p\theta)_L/c_v$.

The wall-normal distributions at synchronization location are reported in figure 13. To second order, the slow mode experiences a local decrease of perturbation kinetic energy in the subsonic near-wall region (i.e. $\hat{p}\hat{\theta} < 0$). On the contrary, the pressure–dilatation contribution to the perturbation kinetic energy of mode F is positive ($\hat{p}\hat{\theta} > 0$). Accordingly, for the slow mode, there is a transfer from mechanical to thermal perturbation energy ($p\theta < 0$ and $-\hat{T}(p\theta)_L > 0$), whereas a reversed process is experienced by the fast mode ($\hat{p}\hat{\theta} > 0$ and $-\hat{T}(p\theta)_L < 0$). In the subsonic region $\hat{p}\hat{\theta}$ and $-\hat{T}(p\theta)_L$ are in phase opposition (perturbation kinetic energy is produced through $\hat{p}\hat{\theta}$ at the

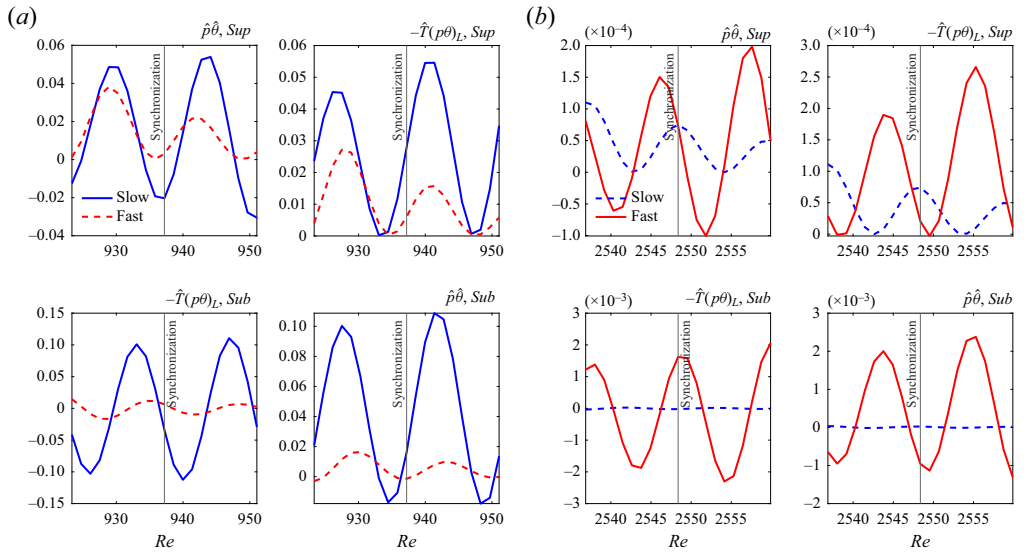

Figure 12. Streamwise distributions of $\hat{p}\hat{\theta}$ and $-\hat{T}(p\theta)_L$ of modes S and F at various wall-normal locations. (*a*) $M = 4.5$; (*b*) $M = 5.5$.

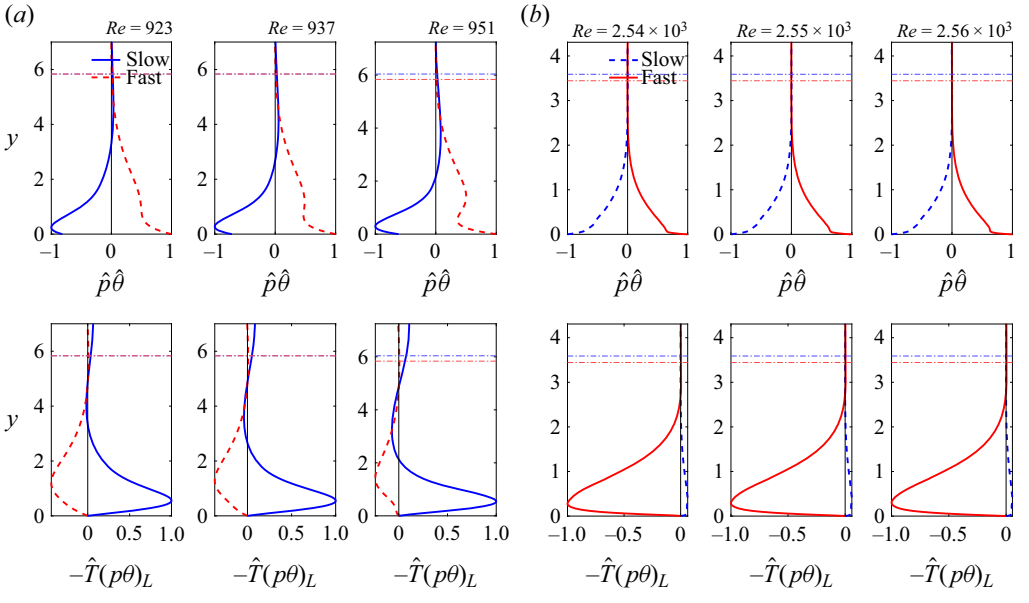

Figure 13. Wall-normal distributions of normalized energy exchange rates due to dilatational effects across synchronization location to second order. The horizontal lines indicate the height of the sonic line for slow and fast modes. (*a*) $M = 4.5$; (*b*) $M = 5.5$.

expense of temperature perturbation energy through term $-\hat{T}(p\theta)_L$ and vice versa). As a consequence, we conclude that when $\hat{p}\hat{\theta} \gtrless 0$, $-\hat{T}\bar{p}\theta \lessgtr 0$, and if $\hat{p}$ and $\hat{\theta}$ are in phase (not in phase), $\hat{T}$ and $\hat{\theta}$ are also in phase (not in phase).

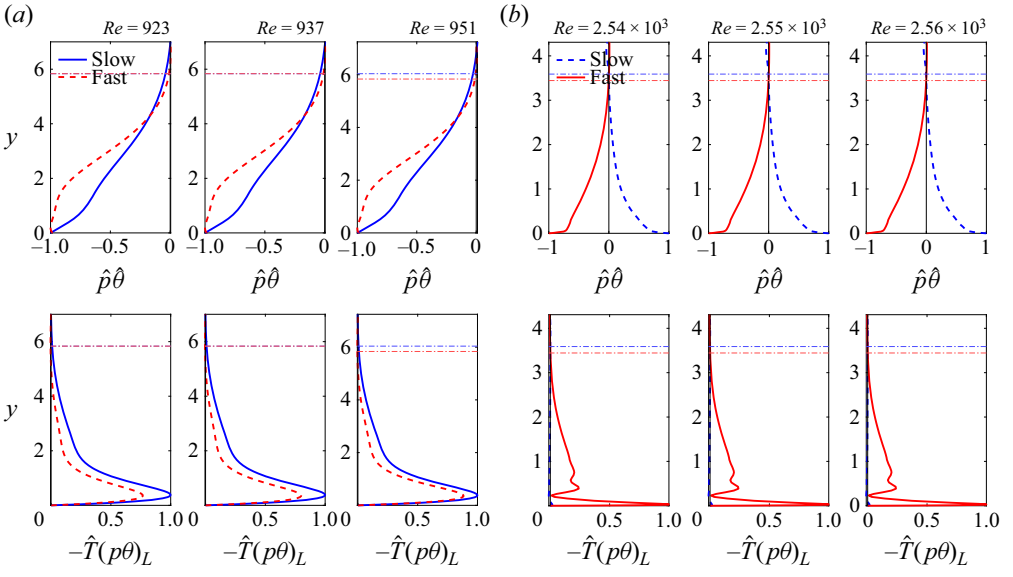

Figure 14. Wall-normal distributions of first-order normalized energy exchange rates due to dilatational effects across synchronization location. (*a*) $M = 4.5$; (*b*) $M = 5.5$.

It is interesting to observe that this bi-directionality is verified also to first order (figure 14). In principle, this result is not to be expected. Indeed, if it is true for the kinetic energy ($u_i^2/2$) and the 'energy variable' ($T^2/2$) of the flow, the same conclusion cannot be reached *a priori* for the perturbation field at any order (i.e. when $\hat{p}\hat{\theta} \gtrless 0$, $-\hat{T}(p\theta)_L$ can take, in principle, any value). In figure 15 we report the wall-normal distributions of $(p\theta)_L$ and $\bar{p}\hat{\theta}$ up to second order. The figure shows that $(p\theta)_L \approx \bar{p}\hat{\theta}$ (i.e. the base flow dilatation is not significant in the establishment of the streamwise evolution of the linearized pressure–dilatation term).

The observed change in sign of the pressure–dilatation indicates that a two-way reversible energy transfer process is established, alternating between cooling and heating in both the streamwise and wall-normal directions. The direction of this conversion process is determined by the sign of the phase difference between the pressure and the dilatation $\cos(\varphi_p - \varphi_\theta)$, φ_p and φ_θ being the phase of p and θ, respectively (Zhu *et al.* 2020, 2021), where

$$\cos(\varphi_p - \varphi_\theta) := \frac{(p\theta)}{p_{rms}\theta_{rms}} \quad \text{with} \quad \begin{cases} p = \bar{p} + \epsilon\mathscr{R}(\hat{p}') + \epsilon^2\mathscr{R}(\hat{p}'') \\ \theta = \bar{\theta} + \epsilon\mathscr{R}(\hat{\theta}') + \epsilon^2\mathscr{R}(\hat{\theta}''). \end{cases} \tag{6.2}$$

Figure 16 shows the streamwise distribution of $\cos(\varphi_p - \varphi_\theta)$ in the subsonic (at $y = y_s/8$) and supersonic (at $y = y_{crit}$) regions across synchronization for $M = 4.5$ and $M = 5.5$. The wall-normal distributions at three different streamwise locations (before, at and past synchronization) are displayed in figure 17. The figures show that in the subsonic region the phase difference $(\varphi_p - \varphi_\theta)$ varies periodically in the streamwise direction assuming positive and negative values, and it is approximately constant in the wall-normal direction. For $M = 4.5$, the initially unstable mode (mode S) experiences mild heating/cooling/heating as it evolves in the near-wall layer and cooling moving away from the wall. Similarly, for $M = 5.5$, the initially unstable mode (mode F) experiences

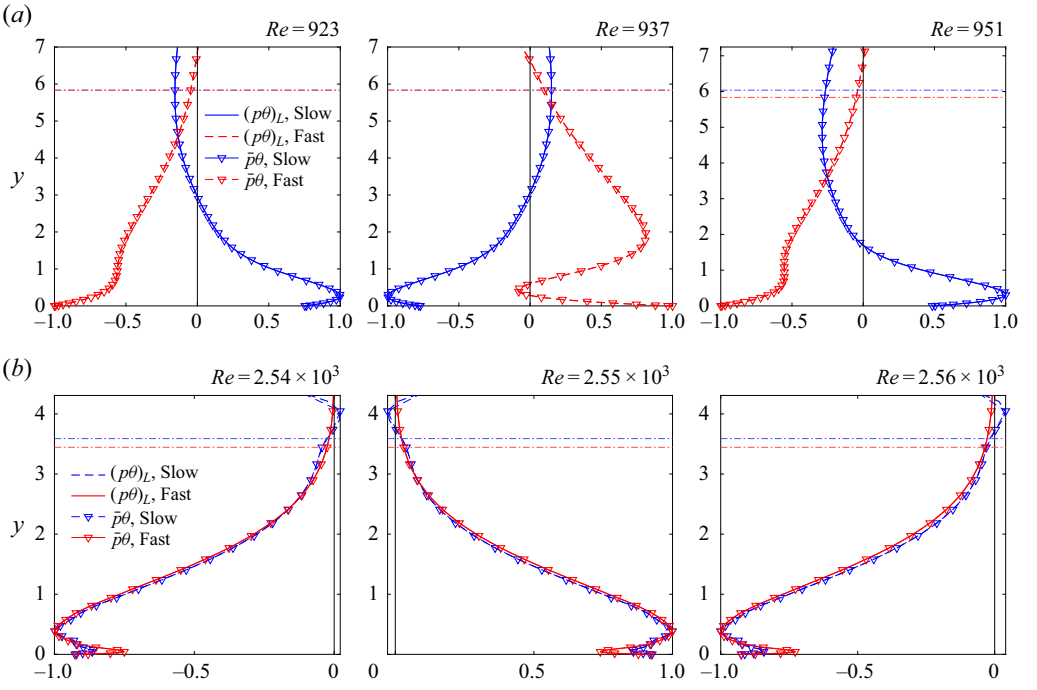

Figure 15. Wall-normal distributions of $(p\theta)_L$ and $\bar{p}\hat{\theta}$ across synchronization location. The horizontal lines indicate the height of the sonic line for slow and fast modes. (*a*) $M = 4.5$; (*b*) $M = 5.5$.

cooling/heating/cooling in the near-wall region and undergoes cooling farther away from the wall. It is also interesting to observe that at first order $(\varphi_p - \varphi_\theta)$ does not vary with x (figure 17), in agreement with the findings of Zhu *et al.* (2020).

The streamwise distributions of ϕ_{S^2} and ϕ_{θ^2} (generically referred to as dissipation rates of the perturbation kinetic energy) and of $\hat{T}\phi_L/c_v$ and ϕ_{k_T} (generically referred to as the generation rates of the temperature perturbation energy) are reported in figure 18. The dissipation and generation rates are normalized, respectively, by the local $\max_x |\hat{p}\hat{\theta}|$ and $\max_x |\hat{T}(p\theta)_L/c_v|$. The figure shows that the dilatational part of the deformation work is smaller than that associated with the deformation tensor (that contributes to local heating, even though negligible). In addition, thermal power dissipation is larger than the linearized viscous dissipation of temperature perturbation energy. As previously observed when discussing the entropy budget, the irreversible exchanges are much smaller than the reversible ones ($\hat{p}\hat{\theta}$ and $-\hat{T}(p\theta)_L/c_v$, not reported in the figure for clarity). It is also interesting to observe that the irreversible energy exchange rates exhibit the same feature as the reversible ones. Namely, the initially unstable modes (the slow and fast modes, respectively, for $M = 4.5$ and $M = 5.5$) undergo an irreversible energy exchange process that grows in amplitude in the streamwise direction, whereas the initially stable modes undergo rapidly decaying energy exchanges.

The streamwise cumulative total perturbation kinetic energy ($\mathcal{I}_{p\theta}$) and temperature perturbation energy ($\mathcal{I}_{-T(p\theta)_L}$) exchanged by dilatation, respectively, in the subsonic (superscript '*sub*') and supersonic (superscript '*sup*') regions are reported in figure 19,

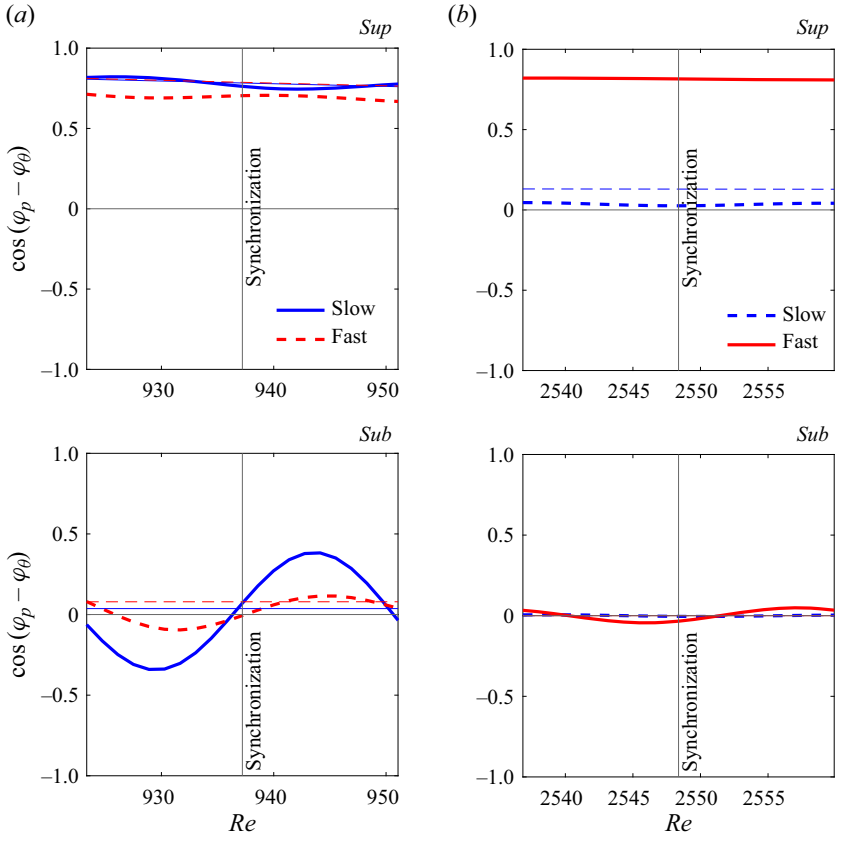

Figure 16. Streamwise distributions of $\cos(\varphi_p - \varphi_\theta)$ at $y = y_{crit}$ (*Sup*) and $y = y_s/8$ (*Sub*). Thin lines, first order; thick lines, up to second order. (*a*) $M = 4.5$; (*b*) $M = 5.5$.

where

$$\left.\begin{aligned} \mathcal{I}^{sub}_{p\theta} &= \int^{x}\int_{0}^{y_s} p\theta \,\mathrm{d}y\,\mathrm{d}x, \quad \mathcal{I}^{sub}_{-T(p\theta)_L} = \int^{x}\int_{0}^{y_s} [-T(p\theta)_L]\,\mathrm{d}y\,\mathrm{d}x, \\ \mathcal{I}^{sup}_{p\theta} &= \int^{x}\int_{y_s}^{\delta} p\theta \,\mathrm{d}y\,\mathrm{d}x, \quad \mathcal{I}^{sup}_{-T(p\theta)_L} = \int^{x}\int_{y_s}^{\delta} [-T(p\theta)_L]\,\mathrm{d}y\,\mathrm{d}x. \end{aligned}\right\} \tag{6.3}$$

In the subsonic and supersonic, regions the terms are normalized by $\int^{x_{end}} |\int_0^{y_s}(\cdot)\,\mathrm{d}y|\,\mathrm{d}x$ and $\int^{x_{end}} |\int_{y_s}^{\delta}(\cdot)\,\mathrm{d}y|\,\mathrm{d}x$, respectively. In both the subsonic and supersonic regions across synchronization, the cumulative total perturbation kinetic energy of the initially unstable modes (mode S for $M = 4.5$ and mode F for $M = 5.5$) exchanged by pressure–dilatation is negative, whereas the cumulative temperature perturbation energy is positive. Namely, unstable modes experience a reduction of kinetic energy while being heated. The linearized pressure–dilatation being driven by the perturbation–dilatation ($(p\theta)_L \approx \bar{p}\hat{\theta}$), pressure and temperature perturbations are in the same relation as the perturbation–dilatation. For the initially stable modes, in the supersonic region an increase of kinetic energy by dilatation effects is not accompanied by a reversible decrease of temperature perturbation energy, and pressure and temperature perturbations are not in the same relation as the perturbation–dilatation. In the subsonic region, as is the case of the

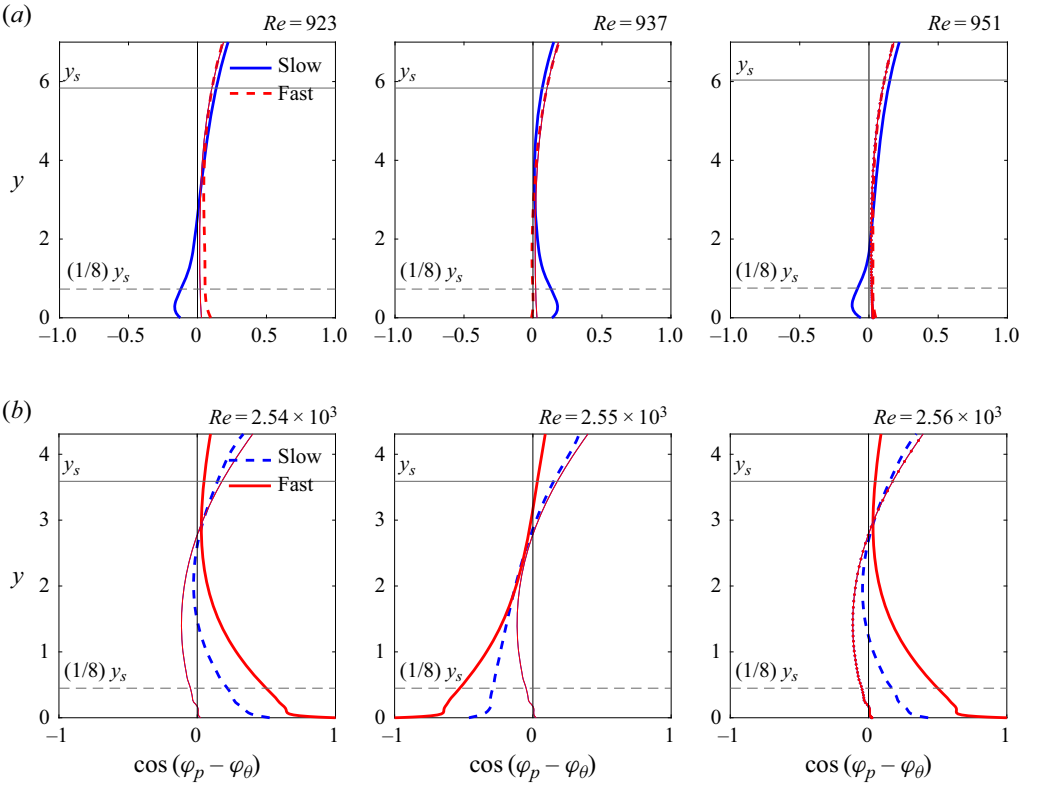

Figure 17. Wall-normal distributions of $\cos(\varphi_p - \varphi_\theta)$ at synchronization location. Thin lines, first order; thick lines, up to second order. (*a*) $M = 4.5$; (*b*) $M = 5.5$.

M	Mode	$\mathcal{I}^{sub}_{p\theta}$	$\mathcal{I}^{sub}_{-T(p\theta)_L}$	$\hat{p}$ and $\hat{T}$	$\mathcal{I}^{sup}_{p\theta}$	$\mathcal{I}^{sup}_{-T(p\theta)_L}$	$\hat{p}$ and $\hat{T}$
4.5	**S**	< 0 (p, θ not in phase)	> 0 (T, θ in phase)	*I*	< 0	> 0	*I*
	F	< 0	> 0	*I*	> 0	> 0	*O*
5.5	S	> 0	< 0	*I*	> 0	> 0	*O*
	F	< 0 (p, θ not in phase)	> 0 (T, θ in phase)	*I*	< 0	> 0	*I*
6	**S**	< 0 (p, θ not in phase)	> 0 (T, θ in phase)	*I*	< 0	> 0	*I*
	F	< 0	> 0	*I*	< 0	> 0	*I*
6.5	**S**	< 0 (p, θ not in phase)	> 0 (T, θ in phase)	*I*	< 0	> 0	*I*
	F	< 0	> 0	*I*	> 0	> 0	*O*

Table 2. Cumulative total energy due to dilatational effects exchanged through self-interaction at synchronization location in the subsonic and supersonic regions at various Mach numbers. Bold indicates initially unstable mode. Here *I* means that $\hat{p}$ and $\hat{T}$ are in phase, whereas *O* means that $\hat{p}$ and $\hat{T}$ are not in phase.

initially unstable modes, they experience a reduction of kinetic energy while being heated. Furthermore, the energy transfer process occurs in the early stages of the evolution and is completed before synchronization location. Table 2 summarizes the results for all Mach numbers and it shows that the energy exchanges exhibit the same features, independently of the Mach number and of the wall thermal conditions.

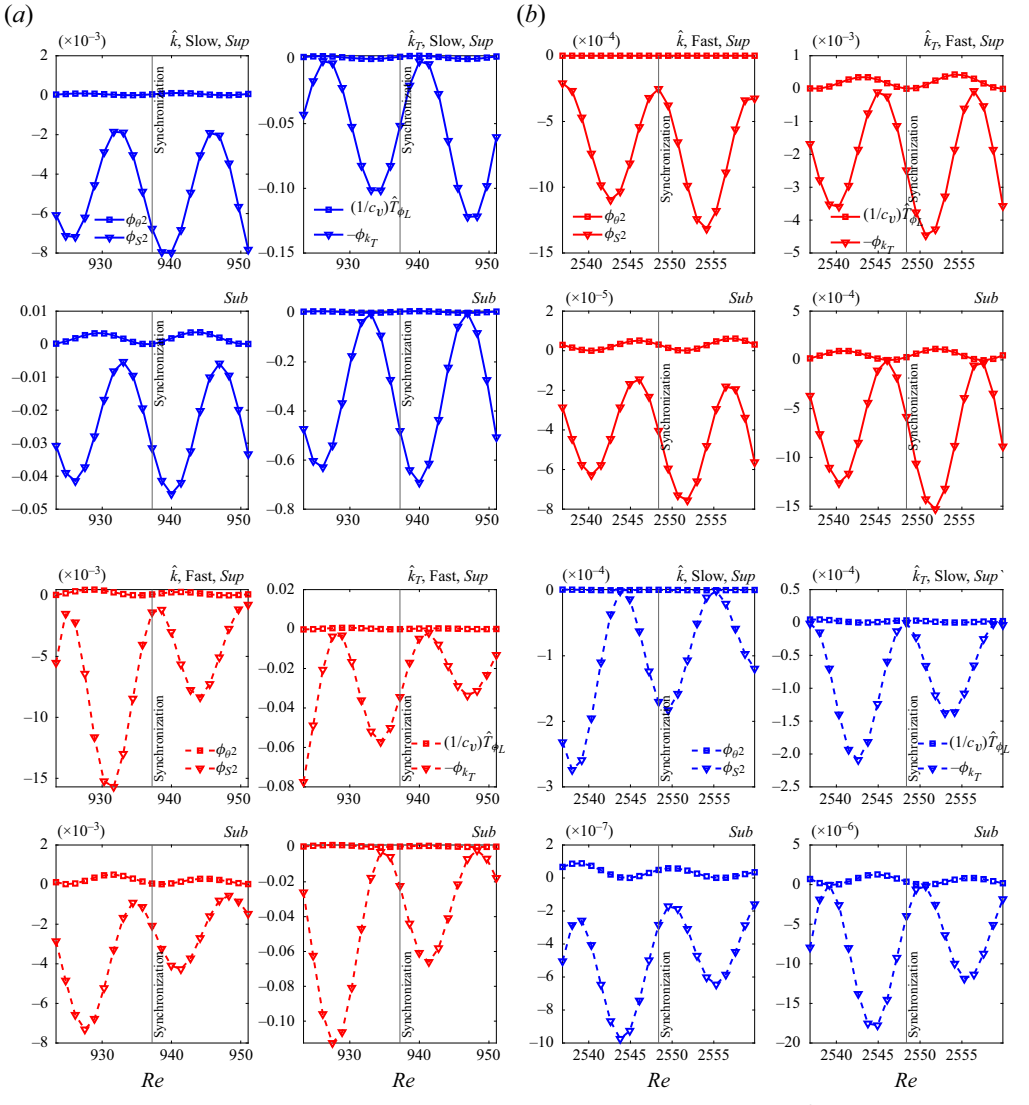

Figure 18. Streamwise distributions of the dissipation (ϕ_{θ^2} and ϕ_{S^2}) and generation ($\hat{T}\phi_L/c_v$ and ϕ_{K_T}) rates experienced by modes S and F at various wall-normal locations. At each y location, the dissipation and generation rates are normalized, respectively, by $\max_x |\hat{p}\hat{\theta}|$ and $\max_x |\hat{T}(p\theta)_L/c_v|$. Solid line, initially unstable mode; dashed line, initially stable mode. (*a*) $M = 4.5$; (*b*) $M = 5.5$.

To further highlight the minor role of cross-interactions, we report in figure 20 the streamwise distributions of the cumulative total perturbation kinetic energy ($\mathcal{J}_{p\theta}$) and temperature perturbation energy ($\mathcal{J}_{-T(p\theta)_L}$) exchanged by cross-interaction (S/F and F/S as defined in § 4.2.4) through dilatation. The results show that the energy exchanges exhibit the same features of self-interactions, independently of the Mach number and of the wall thermal conditions.

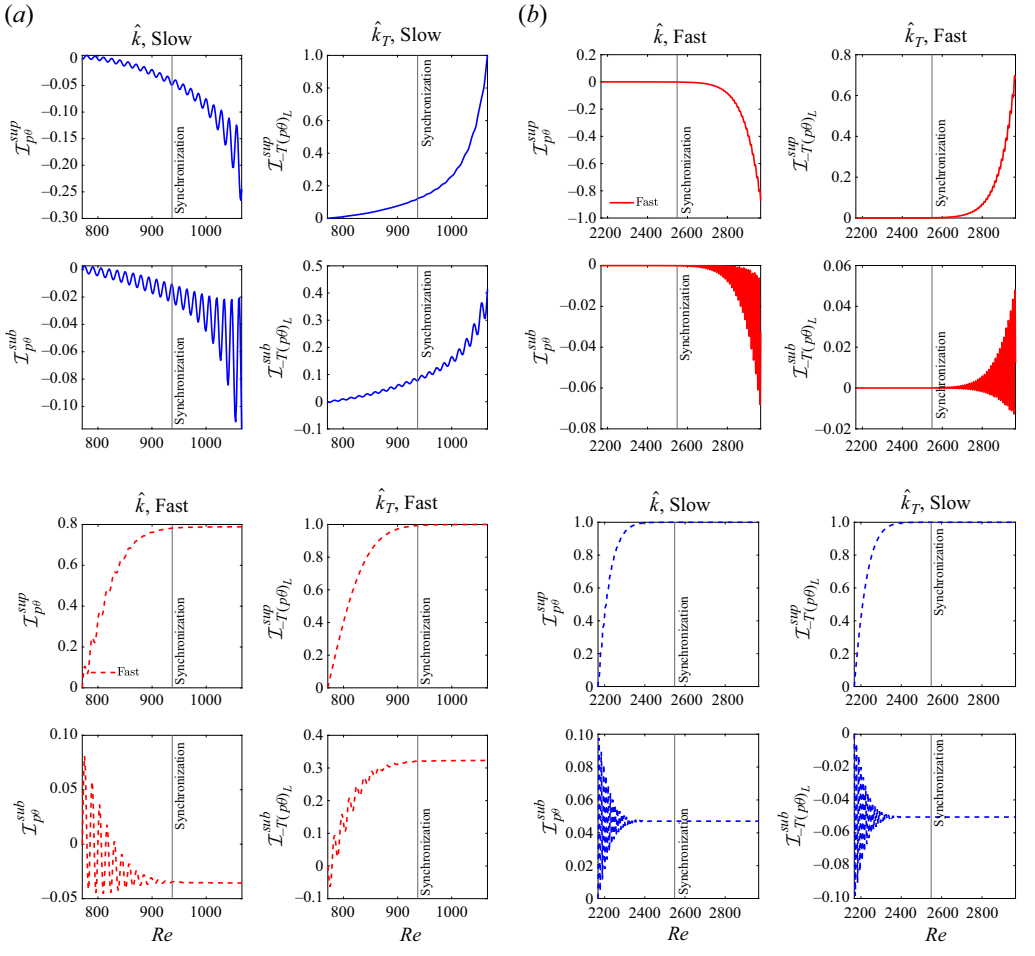

Figure 19. Streamwise distributions of the cumulative total perturbation kinetic energy ($\mathcal{J}_{p\theta}$) and temperature perturbation energy ($\mathcal{J}_{-T(p\theta)_L}$) of modes S and F exchanged through dilatation in the subsonic (superscript '*sub*') and supersonic (superscript '*sup*') regions. In the subsonic and supersonic regions, the rates are normalized, respectively, by $\int^{x_{end}} |\int_0^{y_s} (\cdot)\,\mathrm{d}y|\,\mathrm{d}x$ and $\int^{x_{end}} |\int_{y_s}^{\delta} (\cdot)\,\mathrm{d}y|\,\mathrm{d}x$. Solid line, initially unstable mode; dashed line, initially stable mode. (*a*) $M = 4.5$; (*b*) $M = 5.5$.

7. Conclusions

In the present study we have carried out an analysis of the energy exchange mechanisms driving the evolution of the leading perturbation modes at hypersonic Mach number for both adiabatic and cold-wall thermal conditions. The analysis focusing on the early stages of laminar-to-turbulent transition, we have developed a weakly nonlinear formulation of the hypersonic boundary-layer stability following the work of Chu & Kovasznay (1958).

The selected conditions of the adiabatic wall cases are those of Ma & Zhong (2003*a*) and Reed & Balakumar (1990) for $M = 4.5$ and $M = 6$, respectively, whereas for the cold-wall cases they are those of Fedorov & Tumin (2011) at $M = 5.5$ and $M = 6.5$. Linear stability theory shows that all selected cases exhibit synchronization of the slow (S) and fast (F) modes, and are all inviscidly unstable. For the adiabatic cases and for the $M = 6.5$ cold-wall case, mode S is initially unstable, whereas mode F is the initially unstable one at $M = 5.5$.

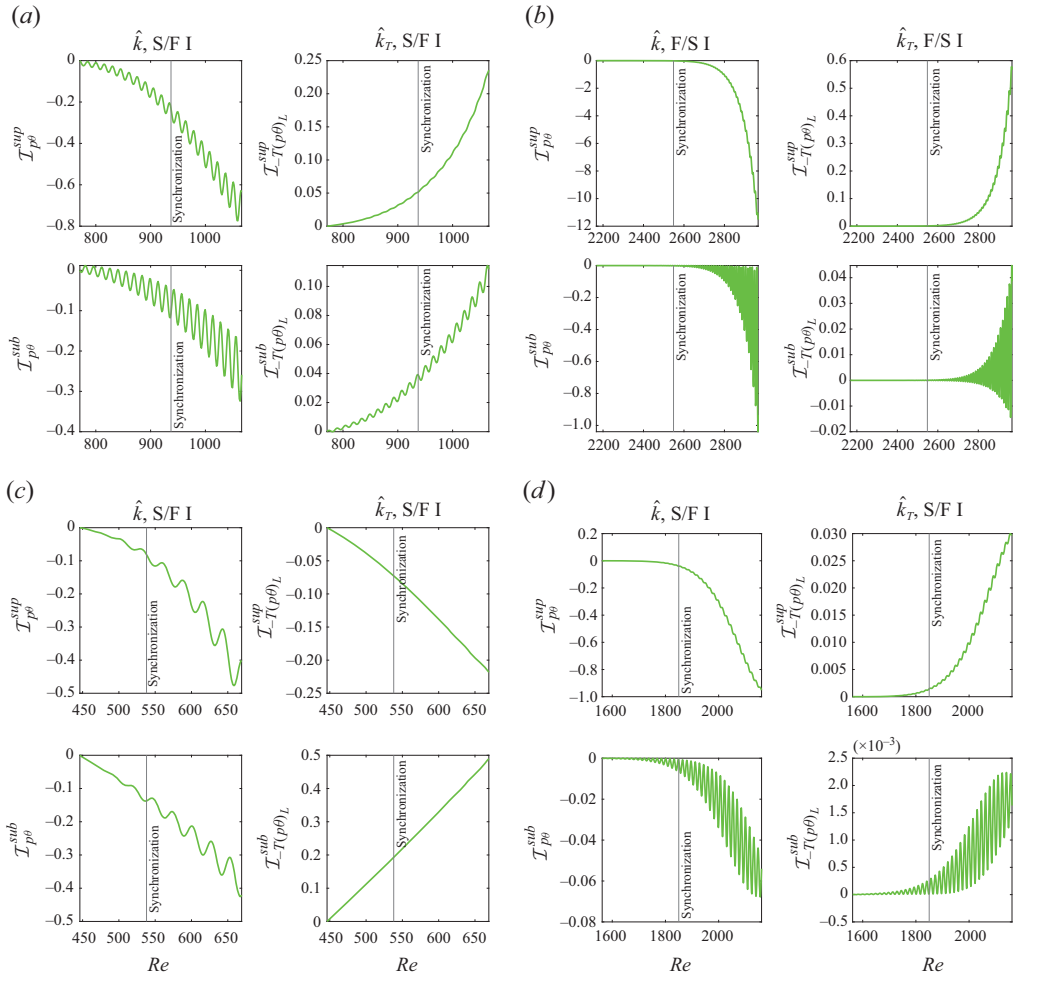

Figure 20. Initially unstable/initially stable mode interactions. Streamwise distributions of the cumulative total perturbation kinetic energy ($\mathcal{I}_{p\theta}$) and temperature perturbation energy ($\mathcal{I}_{-T(p\theta)_L}$) exchanged by cross-interaction (S/F and F/S) through dilatation in the subsonic (superscript '*sub*') and supersonic (superscript '*sup*') regions. In the subsonic and supersonic regions the rates are normalized, respectively, by $\int^{x_{end}} |\int_0^{y_s} (\cdot)\,\mathrm{d}y|\,\mathrm{d}x$ and $\int^{x_{end}} |\int_{y_s}^{\delta} (\cdot)\,\mathrm{d}y|\,\mathrm{d}x$ of the corresponding direct-interaction terms (S/S and F/F, respectively). (*a*) $M = 4.5$, S/F; (*b*) $M = 5.5$, F/S; (*c*) $M = 6$, S/F; (*d*) $M = 6.5$, S/F.

A detailed scrutiny of the budgets of the various perturbation variables, including the perturbation entropy, the perturbation kinetic energy and the temperature perturbation energy, has led us to conclude that there is no dominant physical mechanism leading to synchronization and that the nature of the energy transfer process is essentially inviscid. Perturbation kinetic energy and temperature perturbation energy are reversibly exchanged through perturbation–dilatational effects, the exchanges associated with those due to base flow dilatation being negligible.

The energy transfer mechanism is driven by the initially unstable modes, and their synchronization with the initially stable modes is not the result of any particular mechanism that takes over. The subsonic layer is the region where the energy transfer mechanism is primarily seeded as a consequence of the thermoacoustic trapping. In this

region, the analysis shows that the pressure and temperature perturbations (at any order) are in the same relation as the perturbation–dilatation (of the same order). As a result, when p and θ are in phase, T and θ are also in phase and perturbation kinetic energy is produced at the expense of temperature perturbation energy. The opposite is true when p and θ are not in phase.

The direction of the conversion process associated with $p\theta$ is determined by the sign of the phase difference between the pressure and the dilatation. The phase difference $(\varphi_p - \varphi_\theta)$ features a nearly sinusoidal variation in the streamwise direction alternating between positive and negative values, exhibiting sign changes also in the wall-normal direction in the subsonic region. This indicates that a two-way reversible energy transfer process is established alternating between cooling and heating, in both the streamwise and wall-normal directions. This behaviour is observed only when accounting for second-order contributions, thus confirming the essential role of nonlinear effects in the phase change of the pressure–dilatation.

In the subsonic layer, the thermal power dissipation due to heat conduction is strongly affected by the wall thermal conditions, and is more significant for cold wall due to reduction of the boundary-layer scales and the subsequent increase of both the mean and perturbation temperature gradients. In the supersonic region, the large gradients that establish at the critical layer height account for significant thermal power dissipation independently of the wall thermal state.

In conclusion, the present study indicates that the spatial evolution of both slow and fast modes is driven by the same dilatational mechanisms. The analysis of the amplitudes of the nonlinear contributions for both self- and cross-interactions of first-order velocity and temperature modes shows that no significant changes occur as the modes evolve in the streamwise direction when crossing the synchronization location, and this for both self- and cross-interactions. In addition, we also observe that the energy exchanges exhibit the same features of self-interactions, independently of the Mach number and of the wall thermal conditions. This result is consistent with PSE and DNS analyses that observe only the unstable mode (hence, no cross-interaction). Another possibility to further investigate the absence of FS synchronization at various Mach numbers and wall thermal conditions might be to use an input/output methodology, where modes F and S could be prescribed as inputs, and the output response could rely on DNS or nonlinear PSE solver, rather than the linearized Navier–Stokes solver in Nichols & Candler (2019).

Supplementary material. Supplementary material is available at https://doi.org/10.1017/jfm.2024.912.

Acknowledgements. The first author acknowledges funding received from Princeton University as Global Research Scholar and William Robert Kenan, Jr., Distinguished Visiting Professor in the Department of Mechanical and Aerospace Engineering of the School of Engineering and Applied Science. He also acknowledges fruitful exchanges on the subject with Professor H. A. Stone.

Declaration of interests. The authors report no conflict of interest.

Data availability statement. The data that support the findings of this study are available on request.

Author ORCIDs.
Francesco Grasso https://orcid.org/0000-0003-3826-6624;
Xavier Gloerfelt https://orcid.org/0000-0002-2156-8282.

Appendix A. Governing equations for the base flow properties

A.1. *Base flow equations*

The governing equations for the base flow are derived assuming two-dimensional (quasi-)non-parallel base flow, namely $\bar{u} = \bar{u}(x, y)$, $\bar{v} = \bar{v}(x, y)$, $\bar{w} = 0$, $\bar{\rho} = \bar{\rho}(x, y)$, $\bar{T} = \bar{T}(x, y)$, $\bar{p} = \bar{p}(x, y)$. In non-divergence form, the governing equations (2.1*a*)–(2.1*c*) for the base flow variables $(\bar{\rho}, \bar{u}, \bar{v}, \bar{p}, \bar{T})$ reduce to

$$\bar{u}\frac{\partial \bar{\rho}}{\partial x} + \bar{v}\frac{\partial \bar{\rho}}{\partial y} + \bar{\rho}\frac{\partial \bar{u}}{\partial x} + \bar{\rho}\frac{\partial \bar{v}}{\partial y} = 0, \tag{A1}$$

$$\bar{u}\frac{\partial \bar{u}}{\partial x} + \bar{v}\frac{\partial \bar{u}}{\partial y} = -\frac{1}{\bar{\rho}}\frac{\partial \bar{p}}{\partial x} + D_{\bar{u}}, \tag{A2}$$

$$\bar{u}\frac{\partial \bar{v}}{\partial x} + \bar{v}\frac{\partial \bar{v}}{\partial y} = -\frac{1}{\bar{\rho}}\frac{\partial \bar{p}}{\partial y} + D_{\bar{v}}, \tag{A3}$$

$$\bar{u}\frac{\partial \bar{T}}{\partial x} + \bar{v}\frac{\partial \bar{T}}{\partial y} = -\frac{\bar{p}}{\bar{\rho}c_v}\left(\frac{\partial \bar{u}}{\partial x} + \frac{\partial \bar{v}}{\partial y}\right) + D_{\bar{T}} + \phi_{\bar{T}}, \tag{A4}$$

$$\bar{p} = \bar{\rho}R\bar{T}, \tag{A5}$$

with

$$\begin{aligned} D_{\bar{u}} = {} & \bar{\nu}\frac{\partial}{\partial x}\left[2\frac{\partial \bar{u}}{\partial x} - \frac{2}{3}\left(\frac{\partial \bar{u}}{\partial x} + \frac{\partial \bar{v}}{\partial y}\right)\right] + \bar{\nu}\frac{\partial}{\partial y}\left(\frac{\partial \bar{u}}{\partial y} + \frac{\partial \bar{v}}{\partial x}\right) \\ & + \frac{1}{\bar{\rho}}\left[2\frac{\partial \bar{u}}{\partial x} - \frac{2}{3}\left(\frac{\partial \bar{u}}{\partial x} + \frac{\partial \bar{v}}{\partial y}\right)\right]\frac{\partial \bar{\mu}}{\partial x} + \frac{1}{\bar{\rho}}\left(\frac{\partial \bar{u}}{\partial y} + \frac{\partial \bar{v}}{\partial x}\right)\frac{\partial \bar{\mu}}{\partial y}, \end{aligned} \tag{A6}$$

$$\begin{aligned} D_{\bar{v}} = {} & \bar{\nu}\frac{\partial}{\partial x}\left(\frac{\partial \bar{u}}{\partial y} + \frac{\partial \bar{v}}{\partial x}\right) + \bar{\nu}\frac{\partial}{\partial y}\left[2\frac{\partial \bar{v}}{\partial y} - \frac{2}{3}\left(\frac{\partial \bar{u}}{\partial x} + \frac{\partial \bar{v}}{\partial y}\right)\right] \\ & + \frac{1}{\bar{\rho}}\left(\frac{\partial \bar{u}}{\partial y} + \frac{\partial \bar{v}}{\partial x}\right)\frac{\partial \bar{\mu}}{\partial x} + \frac{1}{\bar{\rho}}\left[2\frac{\partial \bar{v}}{\partial y} - \frac{2}{3}\left(\frac{\partial \bar{u}}{\partial x} + \frac{\partial \bar{v}}{\partial y}\right)\right]\frac{\partial \bar{\mu}}{\partial y}, \end{aligned} \tag{A7}$$

$$\left.\begin{aligned} D_{\bar{T}} &= \frac{\gamma}{Pr}\nu\left(\frac{\partial^2 \bar{T}}{\partial^2 x} + \frac{\partial^2 \bar{T}}{\partial^2 y}\right) + \frac{\gamma}{Pr}\left(\frac{\partial \bar{T}}{\partial x}\frac{\partial \bar{\mu}}{\partial x} + \frac{\partial \bar{T}}{\partial y}\frac{\partial \bar{\mu}}{\partial y}\right), \\ \phi_{\bar{T}} &= \frac{1}{c_v}\bar{\phi}, \end{aligned}\right\} \tag{A8}$$

with $\bar{\phi}$ the viscous dissipation of base flow kinetic energy ($\bar{k} = (\bar{u}^2 + \bar{u})/2$):

$$\bar{\phi} = \bar{\nu}\left[2\left(\frac{\partial \bar{u}}{\partial x}\right)^2 + 2\left(\frac{\partial \bar{v}}{\partial y}\right)^2 + \left(\frac{\partial \bar{u}}{\partial y} + \frac{\partial \bar{v}}{\partial x}\right)^2 - \frac{2}{3}\left(\frac{\partial \bar{u}}{\partial x} + \frac{\partial \bar{v}}{\partial y}\right)^2\right], \tag{A9}$$

and $D_{\bar{u}}$, $D_{\bar{v}}$ and $D_{\bar{T}}$ and $\bar{\phi}$ represent, respectively, the diffusion of the streamwise and wall-normal velocities and the exchange of the base flow internal energy by heat conduction.

The governing equations for the base flow entropy and energy variables are given as follows:

$$\bar{u}\frac{\partial \bar{s}}{\partial x} + \bar{v}\frac{\partial \bar{s}}{\partial y} = D_{\bar{s}} + \phi_{\bar{s},\bar{u}} + \phi_{\bar{s},\bar{T}}, \tag{A10}$$

$$\bar{u}\frac{\partial \bar{k}}{\partial x} + \bar{v}\frac{\partial \bar{k}}{\partial y} = -\frac{1}{\bar{\rho}}\Pi_{\bar{W}} + \frac{1}{\bar{\rho}}\Pi_{\bar{\theta}} + D_{\bar{k}} - \bar{\phi}, \tag{A11}$$

$$\bar{u}\frac{\partial \bar{k}_T}{\partial x} + \bar{v}\frac{\partial \bar{k}_T}{\partial y} = -\frac{1}{\bar{\rho}}\Pi_{\bar{\theta},\bar{T}} + D_{\bar{k}_T} + \bar{\phi}_u - \bar{\phi}_{k_T}, \tag{A12}$$

where $\bar{k}_T = \bar{T}^2/2$ is the base flow 'temperature' energy variable.

The terms $D_{\bar{s}}$, $\phi_{\bar{s},\bar{u}}$ and $\phi_{\bar{s},\bar{T}}$ appearing in (A10) stand for, respectively, the diffusion of base flow entropy associated with heat conduction, and the generation rates due to viscous and thermal power dissipation:

$$\left.\begin{aligned} D_{\bar{s}} &= \frac{\nu}{Pr}\left[\frac{\partial}{\partial x}\left(\frac{1}{\bar{T}}\frac{\partial \bar{T}}{\partial x}\right) + \frac{\partial}{\partial y}\left(\frac{1}{\bar{T}}\frac{\partial \bar{T}}{\partial y}\right)\right] + \frac{1}{Pr}\frac{1}{\bar{\rho}}\left(\frac{\partial \bar{T}}{\partial x}\frac{\partial \bar{\mu}}{\partial x} + \frac{\partial \bar{T}}{\partial y}\frac{\partial \bar{\mu}}{\partial y}\right), \\ \phi_{\bar{s},\bar{u}} &= \frac{1}{c_p}\frac{1}{\bar{T}}\bar{\phi}, \\ \phi_{\bar{s},\bar{T}} &= \frac{\nu}{Pr}\left[\left(\frac{1}{\bar{T}}\frac{\partial \bar{T}}{\partial x}\right)^2 + \left(\frac{1}{\bar{T}}\frac{\partial \bar{T}}{\partial y}\right)^2\right]. \end{aligned}\right\} \tag{A13}$$

The terms $\Pi_{\bar{W}}$, $\Pi_{\bar{\theta}}$, $D_{\bar{k}}$ and $\bar{\phi}$ of (A11) represent, respectively, the pressure work, the pressure–dilatation, the diffusion of the base flow kinetic energy and its dissipation due to viscous effects:

$$\Pi_{\bar{W}} = \left(\frac{\partial \bar{u}\bar{p}}{\partial x} + \frac{\partial \bar{v}\bar{p}}{\partial y}\right), \tag{A14}$$

$$\Pi_{\bar{\theta}} = \bar{p}\left(\frac{\partial \bar{u}}{\partial x} + \frac{\partial \bar{v}}{\partial y}\right), \tag{A15}$$

$$\begin{aligned} D_{\bar{k}} = {} & \bar{\nu}\frac{\partial}{\partial x}\bar{u}\left[2\frac{\partial \bar{u}}{\partial x} - \frac{2}{3}\left(\frac{\partial \bar{u}}{\partial x} + \frac{\partial \bar{v}}{\partial y}\right)\right] + \bar{\nu}\frac{\partial}{\partial y}\left[\bar{u}\left(\frac{\partial \bar{u}}{\partial y} + \frac{\partial \bar{v}}{\partial x}\right)\right] \\ & + \frac{1}{\bar{\rho}}\bar{u}\left[2\frac{\partial \bar{u}}{\partial x} - \frac{2}{3}\left(\frac{\partial \bar{u}}{\partial x} + \frac{\partial \bar{v}}{\partial y}\right)\right]\frac{\partial \bar{\mu}}{\partial x} + \frac{1}{\bar{\rho}}\bar{u}\left(\frac{\partial \bar{u}}{\partial y} + \frac{\partial \bar{v}}{\partial x}\right)\frac{\partial \bar{\mu}}{\partial y} \\ & + \bar{\nu}\frac{\partial}{\partial x}\left[\bar{v}\left(\frac{\partial \bar{u}}{\partial y} + \frac{\partial \bar{v}}{\partial x}\right)\right] \\ & + \frac{1}{\bar{\rho}}\bar{v}\left(\frac{\partial \bar{u}}{\partial y} + \frac{\partial \bar{v}}{\partial x}\right)\frac{\partial \bar{\mu}}{\partial x} + \bar{\nu}\frac{\partial}{\partial y}\bar{v}\left[2\frac{\partial \bar{v}}{\partial y} - \frac{2}{3}\left(\frac{\partial \bar{u}}{\partial x} + \frac{\partial \bar{v}}{\partial y}\right)\right] \\ & + \frac{1}{\bar{\rho}}\bar{v}\left[2\frac{\partial \bar{v}}{\partial y} - \frac{2}{3}\left(\frac{\partial \bar{u}}{\partial x} + \frac{\partial \bar{v}}{\partial y}\right)\right]\frac{\partial \bar{\mu}}{\partial y}. \end{aligned} \tag{A16}$$

Terms $\Pi_{\bar{\theta},\bar{T}}$, $D_{\bar{k}_T}$, $\bar{\phi}_u = \bar{T}\bar{\phi}$ and $\bar{\phi}_{k_T}$ stand for, respectively, the base flow temperature/pressure–dilatation, the diffusion of the base flow energy variable and its

production due to the action of the base flow viscous forces and the thermal power dissipation associated with base flow heat conduction.:

$$\Pi_{\bar{\theta},\bar{T}} = \bar{T}\bar{p}\left(\frac{\partial \bar{u}}{\partial x} + \frac{\partial \bar{v}}{\partial y}\right), \tag{A17}$$

$$D_{\bar{k}_T} = \frac{\gamma}{Pr}\nu\left(\frac{\partial^2 \bar{k}_T}{\partial x^2} + \frac{\partial^2 \bar{k}_T}{\partial y^2}\right) + \frac{\gamma}{Pr}\frac{1}{\bar{\rho}}\left(\frac{\partial \bar{k}_T}{\partial x}\frac{\partial \bar{\mu}}{\partial x} + \frac{\partial \bar{k}_T}{\partial y}\frac{\partial \bar{\mu}}{\partial y}\right), \tag{A18}$$

$$\bar{\phi}_u = \frac{\gamma}{c_v}\bar{T}\bar{\phi}, \tag{A19}$$

$$\bar{\phi}_{k_T} = \frac{1}{c_v}\bar{\nu}\left[\left(\frac{\partial \bar{T}}{\partial x}\right)^2 + \left(\frac{\partial \bar{T}}{\partial y}\right)^2\right]. \tag{A20}$$

A.2. *Base flow analysis*

The solution of the base flow equations (A1)–(A4) is obtained through the similarity solution of a zero-pressure-gradient compressible laminar boundary layer and introducing a generalized coordinate transformation based on the Lees–Dorodnitsyn similarity variables (Anderson 2002), with the streamwise derivatives appearing in the equations being evaluated by finite differencing. In figure 21 (only the $M = 4.5$ adiabatic wall case is reported), we briefly discuss the budgets of the base flow streamwise velocity component ($\bar{u}$), entropy ($\bar{s}$), kinetic energy ($\bar{k}$) and 'temperature' energy ($\bar{k}_T$). In the critical-layer region, the streamwise convection of $\bar{u}$ ($\bar{u}(\partial\bar{u}/\partial x)$) is affected by diffusion and convection normal to the wall ($\bar{v}(\partial\bar{u}/\partial y)$), which depend strongly on the large gradients that establish in this region. Base flow entropy is produced primarily by thermal power due to heat conduction that is then diffused towards the wall balancing entropy production by viscous dissipation. Similarly, in the region around the critical layer, base flow kinetic energy is produced and it diffuses towards the wall balancing the energy removed by viscous dissipation, whereas $\bar{k}_T$ is removed by thermal power dissipation and diffused by heat conduction towards the wall to balance the production due to viscous dissipation.

Appendix B. Linear stability matrices

Dropping the superscripts $()'$ and $()''$ and decomposing the disturbances in normal modes, the stability equations are cast in the following compact matrix form:

$$\boldsymbol{C}\frac{\mathrm{d}^2\hat{\boldsymbol{q}}}{\mathrm{d}y^2} + \boldsymbol{B}\frac{\mathrm{d}\hat{\boldsymbol{q}}}{\mathrm{d}y} + \boldsymbol{A}\hat{\boldsymbol{q}} = (n-1)f\hat{\boldsymbol{N}}, \tag{B1}$$

where $\boldsymbol{A} = \boldsymbol{A}(\alpha, \omega, M, Re; \bar{\rho}, \bar{u}_i, \bar{p}, \bar{T})$, $\boldsymbol{B} = \boldsymbol{B}(\alpha, \omega, M, Re; \bar{\rho}, \bar{u}_i, \bar{p}, \bar{T})$ and $\boldsymbol{C} = \boldsymbol{C}(\alpha, \omega, M, Re; \bar{\rho}, \bar{u}_i, \bar{p}, \bar{T})$ are (5×5) matrices (we recall that $\hat{\boldsymbol{N}}$ is the normal-mode representation of the first-order interaction contribution to the second-order modes). The non-zero coefficients of $\boldsymbol{A}$, $\boldsymbol{B}$ and $\boldsymbol{C}$ are

$$A_{1,1} = \left(\mathrm{i}\bar{\rho}\alpha + \frac{\partial \bar{\rho}}{\partial x}\right), \tag{B2a}$$

$$A_{1,2} = \frac{\partial \bar{\rho}}{\partial y}, \tag{B2b}$$

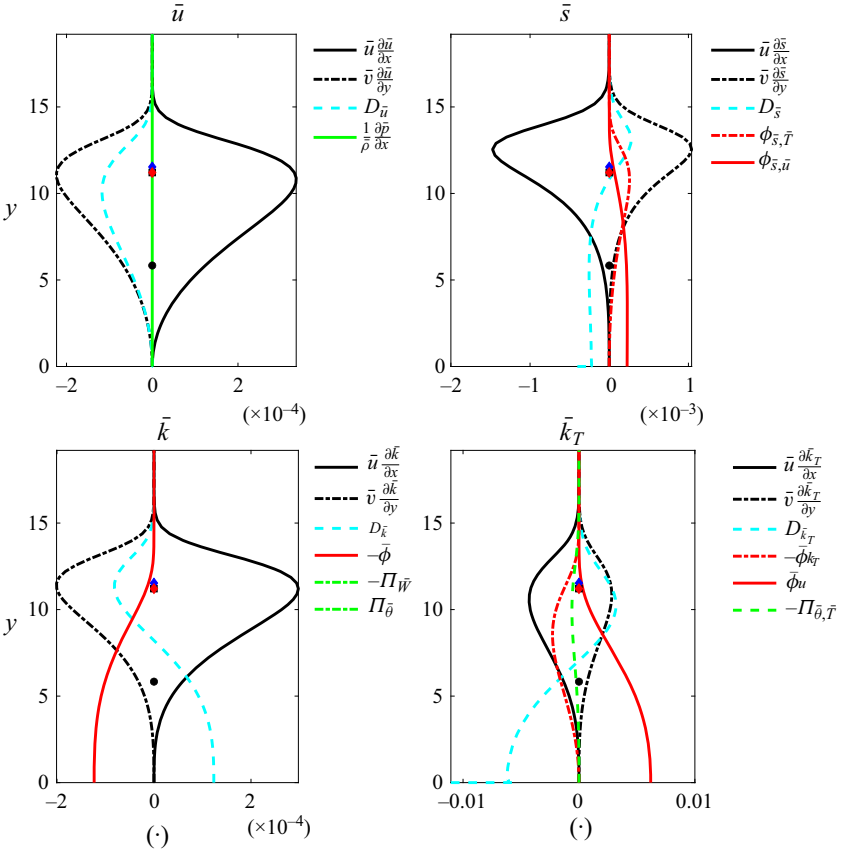

Figure 21. Base flow budgets at $M = 4.5$. The symbols on the vertical axes identify the locations of the sonic and critical layer heights for the slow and fast modes: square, generalized inflection point; diamond, critical layer height; circle, sonic layer height.

$$A_{1,4} = \left\{ \left[\mathrm{i}\,(\alpha\bar{u} - \omega) + \left(\frac{\partial \bar{u}}{\partial x} + \frac{\partial \bar{v}}{\partial y} \right) \right] \frac{\bar{\rho}}{\bar{p}} + \bar{u} \left(\frac{1}{\bar{p}} \frac{\partial \bar{\rho}}{\partial x} - \frac{\bar{\rho}}{\bar{p}^2} \frac{\partial \bar{p}}{\partial x} \right) + \bar{v} \left(\frac{1}{\bar{p}} \frac{\partial \bar{\rho}}{\partial y} - \frac{\bar{\rho}}{\bar{p}^2} \frac{\partial \bar{p}}{\partial y} \right) \right\}, \tag{B2c}$$

$$A_{1,5} = -\left\{ \left[\mathrm{i}\,(\alpha\bar{u} - \omega) + \left(\frac{\partial \bar{u}}{\partial x} + \frac{\partial \bar{v}}{\partial y} \right) \right] \frac{\bar{\rho}}{\bar{T}} + \bar{u} \left(\frac{1}{\bar{T}} \frac{\partial \bar{\rho}}{\partial x} - \frac{\bar{\rho}}{\bar{T}^2} \frac{\partial \bar{T}}{\partial x} \right) + \bar{v} \left(\frac{1}{\bar{T}} \frac{\partial \bar{\rho}}{\partial y} - \frac{\bar{\rho}}{\bar{T}^2} \frac{\partial \bar{T}}{\partial y} \right) \right\}, \tag{B2d}$$

$$A_{2,1} = \left\{ \left[\mathrm{i}\,(\alpha\bar{u} - \omega) + \frac{\partial \bar{u}}{\partial x} \right] \bar{\rho} + \frac{4}{3}\bar{\mu} \left(\alpha^2 - \mathrm{i}\frac{\mathrm{d}\alpha}{\mathrm{d}x} \right) - \frac{4}{3}\mathrm{i}\alpha \frac{\partial \bar{\mu}}{\partial x} \right\}, \tag{B2e}$$

$$A_{2,2} = \left(\bar{\rho} \frac{\partial \bar{u}}{\partial y} - \mathrm{i}\alpha \frac{\partial \bar{\mu}}{\partial y} \right), \tag{B2f}$$

$$A_{2,4} = \left[\left(\bar{u} \frac{\partial \bar{u}}{\partial x} + \bar{v} \frac{\partial \bar{u}}{\partial y} \right) \frac{\bar{\rho}}{\bar{p}} + \mathrm{i}\alpha \right], \tag{B2g}$$

$$A_{2,5} = -\left(\bar{u} \frac{\partial \bar{u}}{\partial x} + \bar{v} \frac{\partial \bar{u}}{\partial y} \right) \frac{\bar{\rho}}{\bar{T}}, \tag{B2h}$$

$$A_{3,1} = \left(\bar{\rho}\frac{\partial \bar{v}}{\partial x} + \frac{2}{3}\mathrm{i}\alpha\frac{\partial \bar{\mu}}{\partial y}\right), \tag{B2i}$$

$$A_{3,2} = \left[\mathrm{i}\left(\alpha\bar{u} - \omega\right) + \frac{\partial \bar{v}}{\partial y}\right]\bar{\rho} + \bar{\mu}\left(\alpha^2 - \mathrm{i}\frac{\mathrm{d}\alpha}{\mathrm{d}x}\right) - \mathrm{i}\alpha\frac{\partial \bar{\mu}}{\partial x}, \tag{B2j}$$

$$A_{3,4} = \left[\left(\bar{u}\frac{\partial \bar{v}}{\partial x} + \bar{v}\frac{\partial \bar{v}}{\partial y}\right)\frac{\bar{\rho}}{\bar{p}}\right], \tag{B2k}$$

$$A_{3,5} = -\left(\bar{u}\frac{\partial \bar{v}}{\partial x} + \bar{v}\frac{\partial \bar{v}}{\partial y}\right)\frac{\bar{\rho}}{\bar{T}}, \tag{B2l}$$

$$A_{4,3} = \left\{\mathrm{i}\left(\alpha\bar{u} - \omega\right)\bar{\rho} + \left[\bar{\mu}\left(\alpha^2 - \mathrm{i}\frac{\mathrm{d}\alpha}{\mathrm{d}x}\right) - \mathrm{i}\alpha\frac{\partial \bar{\mu}}{\partial x}\right]\right\}, \tag{B2m}$$

$$A_{5,1} = \left\{\bar{\rho}\frac{\partial \bar{T}}{\partial x} + \mathrm{i}\alpha\frac{\bar{p}}{c_v} - \mathrm{i}\alpha\frac{\bar{\mu}}{c_v}\left[4\frac{\partial \bar{u}}{\partial x} - \frac{4}{3}\left(\frac{\partial \bar{u}}{\partial x} + \frac{\partial \bar{v}}{\partial y}\right)\right]\right\}, \tag{B2n}$$

$$A_{5,2} = \left[\bar{\rho}\frac{\partial \bar{T}}{\partial y} - \mathrm{i}\alpha\frac{\bar{\mu}}{c_v}2\left(\frac{\partial \bar{u}}{\partial y} + \frac{\partial \bar{v}}{\partial x}\right)\right], \tag{B2o}$$

$$A_{5,4} = \left[\left(\bar{u}\frac{\partial \bar{T}}{\partial x} + \bar{v}\frac{\partial \bar{T}}{\partial y}\right)\frac{\bar{\rho}}{\bar{p}} + \frac{1}{c_v}\left(\frac{\partial \bar{u}}{\partial x} + \frac{\partial \bar{v}}{\partial y}\right)\right], \tag{B2p}$$

$$A_{5,5} = \left\{\mathrm{i}\left(\alpha\bar{u} - \omega\right)\bar{\rho} - \left(\bar{u}\frac{\partial \bar{T}}{\partial x} + \bar{v}\frac{\partial \bar{T}}{\partial y}\right)\frac{\bar{\rho}}{\bar{p}} + \frac{\gamma}{Pr}\bar{\mu}\left(\alpha^2 - \mathrm{i}\frac{\mathrm{d}\alpha}{\mathrm{d}x}\right) - \mathrm{i}\alpha\frac{\gamma}{Pr}\frac{\partial \bar{\mu}}{\partial x}\right\}; \tag{B2q}$$

$$B_{1,2} = \bar{\rho}, \tag{B3a}$$

$$B_{1,4} = \bar{v}\frac{\bar{\rho}}{\bar{p}}, \tag{B3b}$$

$$B_{1,5} = -\bar{v}\frac{\bar{\rho}}{\bar{T}}, B_{2,1} = \left(\bar{\rho}\bar{v} - \frac{\partial \bar{\mu}}{\partial y}\right), \tag{B3c}$$

$$B_{2,2} = \left(-\mathrm{i}\alpha\frac{1}{3}\bar{\mu} + \frac{2}{3}\frac{\partial \bar{\mu}}{\partial x}\right), \tag{B3d}$$

$$B_{3,1} = \left(-\mathrm{i}\frac{1}{3}\alpha\bar{\mu} - \frac{\partial \bar{\mu}}{\partial x}\right), \tag{B3e}$$

$$B_{3,2} = \left(\bar{\rho}\bar{v} - \frac{4}{3}\frac{\partial \bar{\mu}}{\partial y}\right), \tag{B3f}$$

$$B_{3,4} = 1, \tag{B3g}$$

$$B_{4,3} = \left(\bar{\rho}\bar{v} - \frac{\partial \bar{\mu}}{\partial y}\right), \tag{B3h}$$

$$B_{5,1} = -\frac{\bar{\mu}}{c_v}2\left(\frac{\partial \bar{u}}{\partial y} + \frac{\partial \bar{v}}{\partial x}\right), \tag{B3i}$$

$$B_{5,2} = \left\{\frac{\bar{p}}{c_v} - \frac{\bar{\mu}}{c_v}\left[4\frac{\partial \bar{v}}{\partial y} - \frac{4}{3}\left(\frac{\partial \bar{u}}{\partial x} + \frac{\partial \bar{v}}{\partial y}\right)\right]\right\}, \tag{B3j}$$

$$B_{5,5} = \left(\bar{\rho}\bar{v} - \frac{\gamma}{Pr}\frac{\partial \bar{\mu}}{\partial y}\right); \tag{B3k}$$

$$C_{2,1} = -\bar{\mu}, \tag{B4a}$$

$$C_{3,2} = -\frac{4}{3}\bar{\mu}, \tag{B4b}$$

$$C_{4,3} = -\bar{\mu}, \tag{B4c}$$

$$C_{5,5} = -\frac{\gamma}{Pr}\bar{\mu}. \tag{B4d}$$

References

Anderson, J.D. 2002 *Modern Compressible Flow: With Historical Perspective*, 3rd edn. McGraw-Hill.

Balakumar, P. & Malik, M.R 1992 Discrete modes and continuous spectra in supersonic boundary layers. *J. Fluid Mech.* **239**, 631–656.

Chen, X., Zhu, Y. & Lee, C. 2017 Interactions between second mode and low-frequency waves in a hypersonic boundary layer. *J. Fluid Mech.* **820**, 693–735.

Chen, Y., Guo, P. & Wen, C. 2023*a* Consistent energy-based framework of amplification mechanims for the second mode in hypersonic boundary layers. *Phys. Fluids* **366**, 124107.

Chen, Y., Guo, P. & Wen, C. 2023*b* A unified explanation of energy growth sources for unstable modes in flat-plate boundary layers. *J. Fluid Mech.* **972**, A5.

Chu, B.-T. & Kovasznay, L.S.G. 1958 Non-linear interactions in a viscous heat-conducting compressible gaz. *J. Fluid Mech.* **3**, 494–514.

Doak, P.E. 1971 On the interdependence between acoustic and turbulent fluctuating motions in a moving fluid. *J. Sound Vib.* **19** (2), 211–225.

Doak, P.E. 1989 Momentum potential theory of energy flux carried by momentum fluctuations. *J. Sound Vib.* **131** (1), 67–90.

Fedorov, A. 2011 Transition and stability for high-speed boundary layers. *Annu. Rev. Fluid Mech.* **43**, 79–95.

Fedorov, A. & Tumin, A. 2011 High-speed boundary-layer instability: old terminilogy and a new framework. *AIAA J.* **49** (8), 1647–1657.

Fedorov, A.V. & Khokhlov, A.P. 2001 Prehistory on instability in a hypersonic boundary layer. *Theor. Comput. Fluid Dyn.* **14**, 339–375.

Gill, A.E. 1965 Instabilities of top-hat jets and wakes in compressible fluids. *Phys. Fluids* **8** (8), 1428–1430.

Gloerfelt, X. & Robinet, J.-C. 2017 Silent inflow condition for turbulent boundary layers. *Phys. Rev. Fluids* **2**, 124603.

Kuehl, J.J. 2018 Thermoacoustic interpretation of second-mode instability. *AIAA J.* **56** (9), 3585–3592.

Lees, L. & Lin, C.C. 1946 Investigation of the stability of the laminar boundary layer in a compressible fluid. *NACA Tech. Rep.* 1115.

Liang, T., Kafle, S., Amin Khan, A., Paredes, P. & Kuehl, J. 2023 On the inviscid energetics of Mack's first mode instability. *Theor. Comput. Fluid Dyn.* **37**, 1–15.

Lifshitz, Y., Degani, D. & Tumin, A. 2012 Study of discrete modes branching in high-speed boundary layers. *AIAA J.* **50** (10), 2202–2210.

Ma, Y. & Zhong, X. 2003*a* Receptivity of a supersonic boundary layer over a flat plate. Part 1. Wave structures and interactions. *J. Fluid Mech.* **488**, 31–78.

Ma, Y. & Zhong, X. 2003*b* Receptivity of a supersonic boundary layer over a flat plate. Part 2. Receptivity to free-stream sound. *J. Fluid Mech.* **488**, 79–121.

Mack, L.M. 1963 The inviscid stability of the compressible laminar boundary layer. In *Space Programs Summary*, vol. 37-23, p. 297. Jet Propulsion Laboratory.

Mack, L.M. 1984 Boundary layer linear stability theory. *Tech. Rep.* 709. AGARD.

Miles, J.W. 1957 On the reflection of sound at an interface of relative motion. *J. Acoust. Soc. Am.* **29** (2), 226–228.

Morkovin, M.V. 1987 Transition at hypersonic speeds. *NASA Contractor Rep.* ICASE 178315. NASA Langley Research Center.

Nichols, J.W. & Candler, G.V. 2019 Input-output analysis of complex hypersonic boundary layers. *AIAA SciTech Forum, AIAA Paper* 2020-1383.

Reed, H.L. & Balakumar, P. 1990 Compressible boundary-layer stability theory. *Phys. Fluids* A **2** (8), 1341–1349.

Ribner, H.S. 1957 Reflection, transmission, and amplification of sound by a moving medium. *J. Acoust. Soc. Am.* **29** (4), 435–441.

Stetson, K.F. & Kimmel, R.L. 1992 On hypersonic boundary-layer stability. *AIAA Paper* 92-0737.

TAM, C.K.W. & HU, F.Q. 1989 On the three families of instability waves of high-speed jets. *J. Fluid Mech.* **201**, 447–483.

TIAN, X. & WEN, C. 2021 Growth mechanisms of second-mode instability in hypersonic boundary layers. *J. Fluid Mech.* **908**, R4.

TUMIN, A. 2007 Three-dimensional spatial normal modes in compressible boundary layers. *J. Fluid Mech.* **586**, 295–322.

TUMIN, A. 2020 LST and the eigenfunction expansion method for linearized Navier–Stokes equations - a summary. *AIAA SciTech Forum, AIAA Paper* 2020-0105.

UNNIKRISHNAN, S. & GAITONDE, D.V. 2019 Interactions between vortical, acoustic and thermal components during hypersonic transition. *J. Fluid Mech.* **868**, 611–647.

ZHANG, Y., GÖRTZ, S. & OBERLACK, M. 2022 Over-reflection of acoustic waves by supersonic exponential boundary layer flows. *J. Fluid Mech.* **945**, A9.

ZHONG, X. & WANG, X. 2012 Direct numerical simulation on the receptivity, instability, and transition of hypersonic boundary layers. *Annu. Rev. Fluid Mech.* **44**, 527–561.

ZHU, Y., CHEN, X., WU, J., CHEN, S., LEE, C. & GAD-EL HAK, M. 2018*a* Aerodynamic heating in transitional hypersonic boundary layers: role of second-mode instability. *Phys. Fluids* **30**, 011701.

ZHU, Y., GU, D., ZHU, W., CHEN, S., LEE, C. & ORAN, E.S. 2021 Dilatational-wave-induced aerodynamic cooling in transitional hypersonic boundary layers. *J. Fluid Mech.* **911**, A36.

ZHU, Y., LEE, C., CHEN, X., WU, J., CHEN, S. & GAD-EL HAK, M. 2018*b* New identified principle for aerodynamic heating in hypersonic flows. *J. Fluid Mech.* **855**, 152–180.

ZHU, Y., ZHANG, C., CHEN, X., YUAN, H., WU, J., CHEN, S., LEE, C. & GAD-EL HAK, M. 2016 Transition in hypersonic boundary layers: role of dilatational waves. *AIAA J.* **54** (10), 3039–3049.

ZHU, Y., ZHU, W., GU, D., CHEN, S., LEE, C. & ORAN, E.S. 2020 Acoustic-wave-induced cooling in onset of hypersonic turbulence. *Phys. Fluids* **32**, 061702.